

This discussion paper is/has been under review for the journal The Cryosphere (TC).
Please refer to the corresponding final paper in TC if available.

Assessment of heat sources on the control of fast flow of Vestfonna Ice Cap, Svalbard

M. Schäfer¹, F. Gillet-Chaulet², R. Gladstone¹, R. Pettersson³, V. A. Pohjola³,
T. Strozzi⁴, and T. Zwinger⁵

¹Arctic Centre, University of Lapland, Rovaniemi, Finland

²Laboratoire de Glaciologie et Géophysique de l'Environnement (LGGE), UMR5183,
UJF-Grenoble 1, CNRS, Grenoble, France

³Department of Earth Sciences, Air, Water and Landscape science, Uppsala University,
Uppsala, Sweden

⁴Gamma Remote Sensing and Consulting AG, Gümligen, Switzerland

⁵CSC – IT Center for Science Ltd., Espoo, Finland

Received: 8 September 2013 – Accepted: 22 September 2013 – Published: 15 October 2013

Correspondence to: M. Schäfer (smartina.ac@gmx.de)

Published by Copernicus Publications on behalf of the European Geosciences Union.

Title Page

Abstract

Introduction

Conclusions

References

Tables

Figures

◀

▶

◀

▶

Back

Close

Full Screen / Esc

Printer-friendly Version

Interactive Discussion



Abstract

The dynamic regime of Svalbard's Nordaustlandet ice caps is dominated by fast flowing outlet glaciers, making assessment of their response to climate change challenging. A key element of the challenge lies in the fact that the motion of fast outlet glaciers occurs largely through basal sliding, and is governed by physical processes at the glacier bed, processes that are difficult both to observe and to simulate. Up to now, most of the sliding laws used in ice flow models were based on uniform parameters with a condition on temperature to identify regions of basal sliding. However these models are usually not able to reproduce observed velocities with sufficient accuracy. With the development of inverse methods, it is now common to infer a spatially varying field of sliding parameters from surface ice-velocity observations. These parameter distributions usually reflect a high spatial variability and represent valuable information to understand and test various hypotheses on physical processes involved in sliding. However, in these models, basal sliding is uncoupled from the thermal regime of basal ice and the evolution of the sliding parameters in prognostic simulations remains problematic.

Here we explore the role of different heat sources (friction heating, strain heating and latent heat through percolation of melt water) on the development of sliding and fast flow through thermomechanical coupling on Nordaustlandet outlet glaciers. We focus on Vestfonna with a special emphasis on Franklinbreen, a fast flowing outlet glacier which has been observed to accelerate between 1995 and 2008 and possibly already prior to 1995. We try to reconcile the impacts of temperature and heat sources on basal friction coefficients inferred from observed surface velocities during these two periods.

Our simulations reproduce a temperature profile from borehole measurements, allowing an interpretation of the vertical temperature structure in terms of temporal evolution of climate. We identify firn heating as a crucial heat source to explain Vestfonna's temperature distribution, especially in the thick areas in the center. However, friction heating is the dominant heat source at the bed of fast flowing outlet glaciers. Our findings do not support a purely temperature dependent sliding law for Vestfonna, implying

TCD

7, 5097–5145, 2013

Heat production sources and dynamics of VSF

M. Schäfer et al.

Title Page

Abstract

Introduction

Conclusions

References

Tables

Figures

◀

▶

◀

▶

Back

Close

Full Screen / Esc

Printer-friendly Version

Interactive Discussion



that hydrology and/or sediment physics need to be represented in order to simulate fast flowing outlet glaciers.

1 Introduction

Recent studies suggest that contributions to sea level change over the coming decades will be dominated by cryospheric mass loss in the form of discharge from fast flowing ice streams or outlet glaciers (Meier et al., 2007; Moon et al., 2012; Jacob et al., 2012; Tidewater Glacier Workshop Report, 2013). Therefore, understanding the response of fast flowing features to changing climate is crucial in order to make reliable projections (Moore et al., 2011; Rignot et al., 2011; Shepherd et al., 2012; Dunse et al., 2012).

Observations dating back several decades show multiple modes of fast ice flow behavior including permanently fast flowing outlet glaciers or ice streams, networks of ice streams that switch between fast and slow flow (Boulton and Jones, 1979), pulsing glaciers (Mayo, 1978), natural variability in fast flowing outlet glaciers (Iken, 1981), and surging glaciers that show occasional massive accelerations from a more or less stagnant state. Given that the underlying processes behind this range of features are not yet fully understood, and may show significant overlap, we do not limit consideration to a subset of these possible fast flow behaviors. In the current study, we use the term *fast flow feature* to describe a glacier or ice stream that is capable of flowing significantly faster than can be accounted for by internal deformation – even close to pressure melting point, i.e. that undergoes some form of basal sliding. Note that by *basal sliding* we mean non-zero ice velocity at the bed, which could be caused by sliding over the bed and/or deformation of underlying sediment.

We focus our study on the fast flow features of the Vestfonna ice cap. Austfonna and Vestfonna are the two major ice caps of Nordaustlandet, the second largest island of Svalbard, an Arctic archipelago located at around 80° N. Vestfonna covers about 2400 km² and reaches an elevation of 615 m a.s.l. in its center. Compared to the neighboring Austfonna ice cap Vestfonna has a relatively small area of thick slow moving

Heat production sources and dynamics of VSF

M. Schäfer et al.

Title Page

Abstract

Introduction

Conclusions

References

Tables

Figures



Back

Close

Full Screen / Esc

Printer-friendly Version

Interactive Discussion



interior ice. It is instead dominated by fast flowing outlet glaciers that extend from the coast to close to the ice divide. All the fast outlet glaciers on Vestfonna are thought to be topographically controlled (Pohjola et al., 2011). Many Svalbard glaciers are of surge-type, typically with a quiescent phase of ~ 100 yr, a surge phase of a few years, and an acceleration during the surge of factor 10 or higher. Svalbard surge mechanisms have often been associated with thermal instabilities (Payne and Dongelmans, 1997; Murray et al., 2000; Fowler et al., 2001, 2010). However, such mechanisms are criticized due to their inability to explain surges of temperate (Alaskan type) glaciers (Murray et al., 2000; Fowler et al., 2001), which are suspected to be mainly hydrologically controlled (Murray et al., 2003). Murray et al. (2003) suggest that at least two different surge mechanisms exist specific to temperate and polythermal glaciers. However, Sund et al. (2009) showed that surges in polythermal glaciers may also be initiated above the melt-freeze boundary on the glacier, raising the possibility of a single surge mechanism for both polythermal and temperate glaciers in which the surge is initiated in the temperate part (Sund et al., 2011).

Although thermomechanical control of ice deformation is relatively well understood today (Payne et al., 2000), the physical processes controlling basal sliding, which have been subject to some investigation (Kamb, 2001), remain to be better understood. Many processes and feedbacks have been suggested, including sub-glacial hydrology (Kamb, 1987; Vaughan et al., 2008; Bougamont et al., 2011; van der Wel et al., 2013), deformation of sub-glacial sediments (Truffer et al., 2000), heat gain from sliding (friction heating) (Fowler et al., 2001; Price et al., 2008), from strain heating (Clarke et al., 1977; Pohjola and Hedfors, 2003; Schoof, 2004) or thermal instabilities (Murray et al., 2000). Payne and Dongelmans (1997) show that streaming flow can arise solely as a consequence of coupled flow and temperature evolution. However, while thermomechanics can account for the existence of fast flowing ice streams and long time scale oscillatory behavior (Hindmarsh, 2009; Van Pelt and Oerlemans, 2012), shorter timescale oscillations require additional feedbacks or alternative mechanisms (Fowler et al., 2010). Common to most of the suggested processes is the concept that

Heat production sources and dynamics of VSF

M. Schäfer et al.

Title Page

Abstract

Introduction

Conclusions

References

Tables

Figures

◀

▶

◀

▶

Back

Close

Full Screen / Esc

Printer-friendly Version

Interactive Discussion



backs between basal sliding and the thermal regime are discussed in Sect. 5 before we conclude in Sect. 6.

2 Research area and observational data

Vestfonna (VSF) is characterized by a varied topography with two main ridges and strongly pronounced fast outlet glaciers. In common with most glaciers in Svalbard VSF is polythermal. VSF was the target of a recent International Geophysical Year (IPY) project (Pohjola et al., 2011), and the observational record extends back to IPY 1957–1958 (Schytt, 1964) when data on surface elevation (using barometer methods) and ice thickness (from seismic surveys) were gathered. One focus of this work is Franklinbreen, the largest outlet glacier, which is situated on the northwestern side of the ice cap and has recently accelerated (Pohjola et al., 2011; Braun et al., 2011).

2.1 Digital elevation models of surface and bedrock topography

For surface elevation the topographic map from the Norwegian Polar Institute (NPI) is used (1 : 100 000, 1990). This is based on aerial photography and completed with the International Bathymetric Chart of the Arctic Ocean (IBCAO Jakobsson et al., 2008) in the sea. The coordinate is in UTM zone 33N, with datum WGS 1984. The bedrock data is a combination of ground-based pulsed radar and airborne radio-echo soundings (Pettersson et al., 2011). The ground-based radar was deployed only in the central part, for safety reasons. The airborne radar did not give good bedrock depth in the thicker central area due to scattering and absorption losses in the ice. The combined data coverage is good except in the south western tip of VSF where errors in the DEM may be significant (discussed further in Sect. 4.1.2).

Heat production sources and dynamics of VSF

M. Schäfer et al.

Title Page

Abstract

Introduction

Conclusions

References

Tables

Figures

⏪

⏩

◀

▶

Back

Close

Full Screen / Esc

Printer-friendly Version

Interactive Discussion



2.2 Remote sensing data of surface velocities

Tandem Phase ERS-1/2 1 day SAR scenes were acquired between December 1995 and January 1996 (1 day interval) and surface ice velocities were calculated using SAR interferometry (InSAR) (henceforth “1995 velocities”, Pohjola et al., 2011; Schäfer et al., 2012). Four ALOS PALSAR scenes were acquired between January 2008 and March 2008 with 46 days time interval and velocities calculated using offset-tracking (henceforth “2008 velocities”, Pohjola et al., 2011). For 2011, an ERS-2 SAR data stack acquired in March/April with a 3 days time interval processed with a combined InSAR and tracking approach similar to the 1995 data (Pohjola et al., 2011) is used (referred as “2011 velocities”, unpublished data). In all cases the vertical components of the velocities have been neglected during the calculation of horizontal velocities.

The velocity error in the InSAR data is 2 cm, which corresponds to 7 myr^{-1} for Tandem ERS-1/2 SAR data (1 day time interval) and 2 myr^{-1} for 3-days ERS-2 SAR data (Dowdeswell et al., 2008). By considering a matching error estimate of 1/10th of a pixel, the precision of offset-tracking is about 10 myr^{-1} for the 2008 ALOS PALSAR data separated by a temporal interval of 46 days (Pohjola et al., 2011). In the 2011 ERS-2 data set, dual-azimuth offset-tracking was considered in the northern part of Vestfonna and here the matching error is estimated to be about 35 myr^{-1} ; in the southern part SAR data of only one orbit is available and the error of range-azimuth offset tracking is larger, on the order of 130 myr^{-1} .

The 2008 and 2011 data sets do not cover the ice cap completely, and data gaps have been filled by interpolation and smoothing, except for the south-western corner (a region of slow flow), where the 1995 data were used to fill a larger data gap (neglecting possible variations in Gimlereen).

The surface velocities are presented in Fig. 1 (before interpolation and patching). We observe in all three data sets the two very different flow regimes: slow ice flow over the central area of the ice cap and high velocities in the outlet glaciers. Between 1995 and 2008 a net speed-up in the Franklinreen outlet can be seen. From 2008 to 2011 no

TCD

7, 5097–5145, 2013

Heat production sources and dynamics of VSF

M. Schäfer et al.

Title Page

Abstract

Introduction

Conclusions

References

Tables

Figures

◀

▶

◀

▶

Back

Close

Full Screen / Esc

Printer-friendly Version

Interactive Discussion



large changes occurred, though on Franklinbreen the southern branch continued to accelerate slightly, while the northern branch decelerated. The speed up of Franklinbreen, the flow feature showing the biggest change since 1995 (reaching speeds comparable to other fast flowing outlet glaciers in 2008/2011), is modest compared to other Svalbard surging glaciers (Hagen et al., 1993).

2.3 Thermal boundary conditions

Different thermal boundary conditions are required in the model, one being surface or air temperature. Svalbard's climate has a maritime character with cooler summers and warmer winters than is typical at such a high latitude (Möller et al., 2011). Mean monthly air temperatures on VSF still do not exceed +3 °C, and winter monthly means fall between -10 °C and -15 °C with minimum values of the order of -25 °C to -40 °C (Möller et al., 2011). A lapse rate approach is used in the current study to prescribe the surface temperatures

$$T_{\text{surf}}(\mathbf{x}) = T_{\text{sea}}(\mathbf{x}) - \gamma S(\mathbf{x}) \quad (1)$$

at the surface elevation $S(\mathbf{x})$. We use a lapse rate $\gamma = 0.004 \text{ K m}^{-1}$ (Wadham and Nuttall, 2002; Wadham et al., 2006; Schuler et al., 2007a). This value is close to the one adopted in other studies: $\gamma = 0.0044 \text{ K m}^{-1}$ (Pohjola et al., 2002); Liljequist (1993) found a slightly larger lapse rate of $\gamma = 0.005 \text{ K m}^{-1}$ from measurements between the summit of Vestfonna (known as Ahlmann summit) and the 1957/58 IGY station at Kinnvika. Comparison with data from the atmospheric model WRF (Skamarock et al., 2008; Hines et al., 2011) during 1989–2010 confirms this approach, since a mean lapse rate of 0.0042 K m^{-1} with variations up to 30 % corresponding to up to 1 K in the different directions (B. Claremar Uppsala, personal communication, 2013) is found. We estimate the mean air temperature at sea level, $T_{\text{sea}}(\mathbf{x})$, with the same lapse rate approach from data collected during 2005 to 2009 at various weather stations on Austfonna and Vestfonna (Schuler et al., 2007b; Möller et al., 2011) and find a mean annual temperature of -7.7 °C and a mean winter temperature of -14.5 °C at sea-level.

Heat production sources and dynamics of VSF

M. Schäfer et al.

Title Page

Abstract

Introduction

Conclusions

References

Tables

Figures

◀

▶

◀

▶

Back

Close

Full Screen / Esc

Printer-friendly Version

Interactive Discussion



Heat production sources and dynamics of VSF

M. Schäfer et al.

Title Page

Abstract

Introduction

Conclusions

References

Tables

Figures

◀

▶

◀

▶

Back

Close

Full Screen / Esc

Printer-friendly Version

Interactive Discussion



In addition, the geothermal heat flux is an important basal boundary condition. Contrary to Schäfer et al. (2012) who assumed a geothermal heat flux of 63 mW m^{-2} typical for post-Precambrian, non-orogenic tectonic regions (Lee, 1970), we take the value of 40 mW m^{-2} , which is motivated by the measured gradients of profiles obtained by deep drilling on the Nordaustlandet ice caps (Zagorodnov et al., 1989; Ignatieva and Macheret, 1991; Motoyama et al., 2008). In the case of Nordaustlandet, ground surface temperature changes in the uppermost 1–2 km of the bedrock are most likely still influenced by the cold of the Weichselian period, explaining this lower measured value of 40 mW m^{-2} and leading to good simulations of an observed (via deep drilling) temperature profile on VSF (Motoyama et al., 2008), as explained in Sect. 4.2.

3 Model description

Here only the most relevant equations of the model are presented. The dynamics of the forward model are described in Sect. 3.1 (and further details including some parameter values in the Appendix A). The heat transfer equation and the different heat sources are detailed in Sect. 3.2. In Sect. 3.3 the inverse method applied to infer the basal friction coefficient β is summarized. Finally in Sect. 3.4 the mesh is presented.

The model equations are solved numerically with the Elmer/Ice model. It is based on the open-source multi-physics package Elmer developed at the CSC – IT Center for Science in Espoo, Finland, and uses the finite-element method (Zwinger et al., 2007; Gagliardini and Zwinger, 2008; Gagliardini et al., 2013).

3.1 Forward model

The ice is modeled as a non-linear viscous incompressible fluid flowing under gravity over a rigid bedrock. The force balance (quasi static equilibrium) is expressed by the Stokes equations. The deviatoric stresses $\boldsymbol{\tau}'$ and their second invariant τ_2 are linked to

the strain rates $\dot{\epsilon}$ through Glen's law, which in index notation reads

$$\dot{\epsilon}_{ij} = A(T)\tau_{*}^2\tau'_{ij}. \quad (2)$$

The temperature dependency of the deformation rate factor, $A(T)$, is described by an Arrhenius law

$$A(T) = A_0 \exp(-Q/[R(273.15 + T)]), \quad (3)$$

where R is the universal gas constant, A_0 the prefactor and Q the activation energy. A_0 and Q are given by

$$A_0 = 3.985 \times 10^{-13} \text{Pa}^{-3} \text{s}^{-1}, \quad Q = -60 \text{KJ mol}^{-1}, \quad T \leq -10^\circ\text{C}, \quad (4)$$

$$A_0 = 1.916 \times 10^3 \text{Pa}^{-3} \text{s}^{-1}, \quad Q = -139 \text{KJ mol}^{-1}, \quad T > -10^\circ\text{C} \text{ (Paterson, 1994)}$$

The evolution of free surface S is governed by the kinematic boundary condition

$$\frac{\partial z}{\partial t} + v_x \frac{\partial z}{\partial x} + v_y \frac{\partial z}{\partial y} = v_z + a \text{ on } S, \quad (5)$$

where a represents the climate mass balance and $v_{x,y,z}$ the velocity components. S is assumed to be a stress-free surface, i.e. $\boldsymbol{\tau} \cdot \boldsymbol{n} = 0$.

At the lower boundary B , a linear friction law (Weertman type law, Robin type boundary condition Greve and Blatter, 2009) is imposed

$$\boldsymbol{t} \cdot (\boldsymbol{\tau} \cdot \boldsymbol{n}) + \beta(x, y) \boldsymbol{v} \cdot \boldsymbol{t} = 0, \text{ on } B, \text{ leading to } \boldsymbol{v}_{\parallel} = \frac{1}{\beta(x, y)} \boldsymbol{\tau}_{\parallel}, \quad (6)$$

where \boldsymbol{n} and \boldsymbol{t} are normal and tangential unit vectors, β is the basal friction parameter and $\boldsymbol{v}_{\parallel}$ and $\boldsymbol{\tau}_{\parallel}$ are the basal velocity and stress components parallel to the bed. We assume zero basal melting ($\boldsymbol{v} \cdot \boldsymbol{n} = 0$). The basal friction coefficient field $\beta(x, y)$ will be inferred in this study from surface velocities using an inverse method (Sect. 3.3).

At the upper boundary a Dirichlet condition is imposed on T using the parametrization described in Sect. 2.3. At the bed a heat flux is imposed composed of geothermal heat flux, $q_{\text{geo}} = \kappa \text{grad}T \cdot n$, and friction heat $q_f = u_b \tau_b$ (with u_b the sliding velocity and τ_b the basal drag).

5 The volumetric heat source Q comprises strain heat $Q_s = 2\mu\epsilon^*$, where ϵ^* is the second invariant of the strain rate tensor, and latent heat from firn heating Q_l (latent heat released during refreezing of percolating melt water). Q_l is calculated using the P_{max} model of Wright et al. (2007) as used by Zwinger and Moore (2009). Different characteristic shapes of the time averaged temperature-depth profiles $\bar{T}(d)$ in summer and winter are used (Wright et al., 2007):

$$\bar{T}(d) = \left(\frac{d}{d_{\text{ice}}} - 1 \right) (\bar{T}_a - \bar{T}_w) + \bar{T}_a, \text{ in the winter,} \quad (12)$$

$$\bar{T}(d) = \bar{T}_a \left(1 - \frac{(d - d_{\text{ice}})^2}{d_{\text{ice}}^2} \right)^{\frac{1}{2}}, \text{ in the summer,} \quad (13)$$

15 where d is the depth below the surface. There are three free parameters in this firn heating parametrization: \bar{T}_a and \bar{T}_w are the annual and winter mean air temperatures respectively set according to Sect. 2.3. d_{ice} is the typical penetration depth of the annual temperature cycle which is kept as a free parameter and tuned to reproduce the measurements in the deep ice core (Motoyama et al., 2008), see Sect. 4.2.

20 The resulting volume heat source is deduced by the difference of internal energy defined by the difference $\Delta T(d)$ between the seasonal profiles Eqs. (12) and (13)

$$Q_l(d) = c\rho\Delta T(d), \quad (14)$$

and decreases steadily from the surface to the penetration depth.

Title Page	
Abstract	Introduction
Conclusions	References
Tables	Figures
◀	▶
◀	▶
Back	Close
Full Screen / Esc	
Printer-friendly Version	
Interactive Discussion	



3.3 Inverse model

A variational inverse method (Arthern and Gudmundsson, 2010) is used in this study to infer the spatially varying basal friction coefficient $\beta(x, y)$. It is based on the minimization of a cost function when solving the Stokes Equations iteratively with two different sets of boundary conditions. The definition of the cost function and the minimization algorithm follow Gillet-Chaulet et al. (2012) and Jay-Allemand et al. (2011). This approach is similar to Schäfer et al. (2012) but with the addition of a regularization term (Habermann et al., 2012).

The method iteratively applies a Neumann and a Dirichlet condition at the upper free surface. In the Dirichlet problem the Neumann free upper surface condition is replaced by a Dirichlet condition where the observed surface horizontal velocities are imposed

$$\mathbf{v}_{\text{hor}}(\mathbf{x}) = \mathbf{v}_{\text{obs}}(\mathbf{x}), \forall \mathbf{x} \in S, \quad (15)$$

where $\mathbf{v}_{\text{hor}}(\mathbf{x})$ and $\mathbf{v}_{\text{obs}}(\mathbf{x})$ stand respectively for the modeled and observed horizontal surface velocities. In z -direction, $(\boldsymbol{\tau} \cdot \mathbf{n}) \cdot \mathbf{e}_z = 0$ is imposed on S , where \mathbf{e}_z is the unit vector along the vertical. To avoid unphysical negative values, the friction parameter field $\beta(x, y)$ is expressed as $\beta = 10^\alpha$ and the minimization of the cost function is performed with respect to α . The cost function, which expresses the mismatch between the two solutions for the velocity field with different boundary conditions on the upper surface S , is given by

$$J_0(\beta) = \int_S (\mathbf{v}^N - \mathbf{v}^D) \cdot (\boldsymbol{\tau}^N - \boldsymbol{\tau}^D) \cdot \mathbf{n} dA, \quad (16)$$

where the superscripts N and D refer to the solutions of the Neumann and Dirichlet problems, respectively. To avoid unphysical small wavelength variations in α and to ensure to find a stable unique solution, a Tikhonov regularization term J_{reg} penalizing

TCD

7, 5097–5145, 2013

Heat production
sources and
dynamics of VSF

M. Schäfer et al.

Title Page

Abstract

Introduction

Conclusions

References

Tables

Figures

◀

▶

◀

▶

Back

Close

Full Screen / Esc

Printer-friendly Version

Interactive Discussion



the first spatial derivatives of α is added to the total cost function J_{tot}

$$J_{\text{tot}} = J_0 + \lambda J_{\text{reg}}, \quad (17)$$

$$J_{\text{reg}} = \frac{1}{2} \int_B \left(\frac{\partial \alpha}{\partial x} \right)^2 + \left(\frac{\partial \alpha}{\partial y} \right)^2 dA, \quad (18)$$

5 where λ is a positive parameter (see Sect. 4.1.1 for its choice). The minimization of the cost function is thus a compromise between best fit to observations and smoothness of α , determined by the tuning of λ . The minimization algorithm is described by Gillet-Chaulet et al. (2012) and Gagliardini et al. (2013).

3.4 Meshing

10 Anisotropic mesh refinement is now increasingly used in numerical modeling especially with the finite elements method since the mesh resolution is a critical factor. Schäfer et al. (2012) have investigated effects of varying the resolution in the context of this inverse method. Here we use again the mesh established with the fully automatic, adaptive, isotropic surface remeshing procedure Yams (Frey, 2001). A 2-D footprint-mesh
15 was established according to the glacier outline on the 1990 NPI-map and adapted using the metric based on the Hessian matrix of the observed 1995 surface velocities. Horizontal resolution varies between 250 m and 2500 m. Finally the mesh was extruded vertically in 10 equidistant terrain following layers according to the bedrock and surface data. In the simulations involving firn heating, the mesh was extruded vertically
20 in 20 layers with the upper 10 layer thicknesses reducing towards the surface following a power law. The robustness of the total vertical layer number was already verified in (Schäfer et al., 2012), doubling the number of boundary layers also lead to robust results in the runs including firn heating.

4 Simulations

In this section we present the setup of our simulations. In Sect. 4.1 the unfeasibility of an ideal thermo-mechanical spin-up is addressed and we describe our alternative temperature initialization. In the distribution of the basal sliding coefficient regulating the velocity field is determined before a purely mechanical spin-up is conducted (surface relaxation, Sect. 4.1.2). These simulations are thereafter the starting point for simulations to investigate and validate the influence of the different heat sources, especially to calibrate our firn heating parametrization (Sect. 4.2). A short prognostic simulation is also conducted (Sect. 4.3), emulating the observed acceleration of Franklinbreen with different scenarios with the goal to link the corresponding changes in the basal drag coefficient to variations in temperature or other factors.

4.1 System initialization

The inherent problem if starting from a DEM purely on observed data, is that an instantaneous solution for both the mechanical and the thermo-dynamical problems is needed as a starting point. Thermal initial conditions are critical in modeling of poly-thermal glaciers or ice sheets because of the energy storage capacity of ice, the low advection/diffusion rates on the glacier and the strong thermo-mechanical coupling via the ice viscosity. An ideal spin-up would demand a transient run starting from deglaciated conditions with a long enough spin-up time requiring realistic forcing (temperature, mass balance) as well as knowledge of the velocity field. That's because the VSF temperature distribution at any given instant in time is a function of past evolution of the advection, diffusion of heat and heat sources – friction heating being a major heat source and having a strong time dependency for glaciers with time variable velocities. Air temperature and precipitation records exist over a long enough time. However a precise reconstruction of the velocity field of VSF will not be feasible until we can confidently simulate the evolution of fast flowing glaciers.

TCD

7, 5097–5145, 2013

Heat production sources and dynamics of VSF

M. Schäfer et al.

Title Page

Abstract

Introduction

Conclusions

References

Tables

Figures

◀

▶

◀

▶

Back

Close

Full Screen / Esc

Printer-friendly Version

Interactive Discussion



Heat production sources and dynamics of VSF

M. Schäfer et al.

Title Page

Abstract

Introduction

Conclusions

References

Tables

Figures

◀

▶

◀

▶

Back

Close

Full Screen / Esc

Printer-friendly Version

Interactive Discussion



In the absence of such ideal spin-up we assume steady-state for temperature, including the effects of strain heating and friction heating, even though non-steady-state conditions have occurred on VSF between 1995 and 2008, and probably on longer time scales as well. We found characteristic timescales to reach such a steady-state to be of the order of several hundreds of years (not shown in this paper). This will lead to over- or underestimations of the temperature depending on the past state of each outlet glacier. In practice the errors will be largest closest to the bed where friction heat production has greatest effect and will decay away in the interior regions of the ice cap. Seroussi et al. (2013) also addressed the question of thermal initial conditions and came to the conclusion that steady-state temperatures based on present-day conditions are a reasonable good approximation both for calculations of basal conditions and century-scale transient simulations.

Remaining uncertainties in the model initial conditions (including uncertainties in the model parameters as well as the domain geometry), lead to ice flux divergence anomalies (Zwinger and Moore, 2009; Seroussi et al., 2011), resulting in a non-smooth vertical velocity field. Because of the importance of the vertical velocity field for advection of cold ice from the surface, and to smooth out these ice flux divergence anomalies the free surface is relaxed before conducting further transient simulations.

4.1.1 Inverse simulations to derive spatial patterns of the basal friction

The method of Schäfer et al. (2012) is followed with some improvements: correct marine boundary conditions (Eq. 7) are applied, a regularization term in the cost function is added and a better minimization algorithm is used. The simulations to determine the best weight for the regularization term, λ , in Eq. (17) are performed for simplicity with temperature kept fixed to the depth dependent profile (Sect. 3.2) as done by Schäfer et al. (2012). This is justified because of the small temperature dependency as it was shown in Schäfer et al. (2012). The best value λ is determined by the L-curve analysis (Hansen, 2001) from a plot displaying J_{reg} (smoothness of the friction parameter) as

a function of J_0 (match to observations) using the 1995 velocity data. We find J_0 is minimized by setting $\lambda = 10^{5.0}$, which also leads to acceptable smoothness in β .

In a similar way, we conduct inversions for the basal drag with the 2008 and 2011 surface velocity fields (Fig. 2). These runs are conducted also with the 1990 surface DEM, since no complete additional surface DEM is available. Nuth et al. (2010) and Moholdt et al. (2010) have shown from ICESat laser altimetry data that mean elevation changes over VSF were 0.05 myr^{-1} and -0.16 myr^{-1} over the periods 1990 to 2005 and 2003 to 2008 respectively. The changes form a complex spatial pattern on VSF, with local values up to 1 myr^{-1} in the south. It has been shown (Schäfer et al., 2012) that surface variations of this order (or higher) between 1995 and 2008 or 2011 do not significantly affect the drag fields derived from the inverse method. The same value for the λ parameter as well as the same inhomogeneous mesh have been used, the latter to facilitate comparison. The inferred basal drag coefficient distributions clearly reflect the acceleration of Franklinbreen with decreasing values of the friction coefficient β from 1995 to 2008. For the other outlets the general patterns remain similar for the three periods and show only small local variations.

An iteration scheme between inversion and temperature calculation has been tested. The depth dependent temperature profile (Eq. 8) was used in the first inversion for β , then steady-state calculations of the temperature field (accounting for friction and strain heating) and inversions were run alternately. The resulting β distribution reveals small changes compared to keeping the temperature fixed to the depth dependent profile, showing a certain robustness of β towards changes in temperature. Nevertheless, the value of the cost function has been decreased with the iterative scheme (Fig. 3), showing an improved match between observed and computed surface velocities. Convergence of this iteration was assessed through the cost function and stopped once the cost function stabilized. Convergence of the steady-state temperature field was ascertained through visual inspection.

The effect of firn heating on the resulting β distribution has been studied separately. This is motivated both by the need to save computing resource (firn heating simula-

Heat production sources and dynamics of VSF

M. Schäfer et al.

Title Page

Abstract

Introduction

Conclusions

References

Tables

Figures

◀

▶

◀

▶

Back

Close

Full Screen / Esc

Printer-friendly Version

Interactive Discussion



tions require high resolution in the vertical), and because of the greater uncertainties associated with this heat source compared to the others. It causes very little change to β . For further simulations, the distribution of β obtained with the iteration scheme but neglecting firn heating is adopted (Fig. 2).

4.1.2 Surface relaxation

As initial conditions for transient simulations the free surface is relaxed for three years under zero mass-balance. This relaxation simulation was initialized with output from the inversion-temperature iterations. A short time step (0.1 yr) was chosen to guarantee temporal resolution of artificially strong surface changes induced by the remaining uncertainties. Visual inspection of the smoothness and magnitude of the vertical velocity field was used to determine the end of the relaxation procedure.

The largest changes to the mesh (Fig. 4) occur in the southwestern corner and in some outlet glaciers where there is a significant paucity of bedrock radar data (see Pettersson et al., 2011, for radar coverage). In these outlet glaciers it is even unknown whether additional mountain ridges or valleys exist at the bedrock underlying fast flow features, or whether such features are only driven by surface topography. Some other less important changes are visible in northeastern VSF – again in areas with sparsely covered bedrock data.

A more complex spin-up scheme involving an iteration between surface relaxation, inverse method and temperature calculation was also tested for a single combination of surface velocity data and included heat sources in the temperature calculation. This procedure requires huge computational efforts and does not lead to visible improvements in the results (β field, temperature field, and surface corrections) and is hence not used in this work for several different combinations of surface velocity data (3 possibilities) and included heat sources (6 possibilities).

After the relaxation, a final steady-state temperature field was computed. The resulting state is then used as a starting point for the following simulations.

Heat production sources and dynamics of VSF

M. Schäfer et al.

Title Page

Abstract

Introduction

Conclusions

References

Tables

Figures



Back

Close

Full Screen / Esc

Printer-friendly Version

Interactive Discussion



4.2 Influence of different heat sources on the temperature distribution

From the model state described above, the influence of the different heat sources (Sect. 3.2) on the thermal regime of the ice cap are discussed. Results are compared to the temperature profile measured in a drill hole located in the central area of the ice cap at the east end of the summit ridge; see Fig. 5 for the exact location (Motoyama et al., 2008). Figure 6 shows simulated temperature-depth profiles for the various combinations of heat sources at two other locations on Franklinbreen and Frazerbreen, in the ablation and in accumulation areas respectively. Simulated basal temperatures are shown in Fig. 5.

At the location of the drill hole, using only strain and friction heating, the measured temperature profile cannot be reproduced, even close to the bedrock where these heat sources are most effective, Fig. 7 (brown line compared to the data in red). Various simulations with different parameter sets (free parameter d_{ice} , temperature parameters) in our firn heating parametrization have been conducted and two qualitative observations could be made: (1) with constant surface forcing only (close to) equilibrium temperature simulations including firn heating do affect the temperature in vicinity of the bedrock; (2) these quasi equilibrium solutions do not feature the clear inflexion in the temperature profile visible close to the surface in the observed data. Such simulations lead to temperature profiles similar to the blue curve in Fig. 7, the profiles are only shifted to warmer or colder temperatures. The green, cyan and pink curves in the figure illustrate the evolution of the temperature profile during a transient simulation and how the inflexion of the temperature profile is slowly smoothed out and propagated down towards the bedrock when approaching equilibrium. We thus hypothesize that the observed borehole profile results from a succession of two different surface boundary conditions: (1) a low surface temperature and low firn heating over a period long enough to approach equilibrium and (2) a more recent increase in surface temperature and or firn heating. In order to tune the model to match drilling hole observations (Motoyama et al., 2008),

TCD

7, 5097–5145, 2013

Heat production sources and dynamics of VSF

M. Schäfer et al.

Title Page

Abstract

Introduction

Conclusions

References

Tables

Figures

◀

▶

◀

▶

Back

Close

Full Screen / Esc

Printer-friendly Version

Interactive Discussion



we make the hypothesis that boundary condition changes can be represented in our firn heating parametrization by the penetration depth parameter.

This can be motivated by the fact that ice cores elsewhere in Svalbard indicate that firn heating and percolation have been frequent in the last 500–1000 yr (Van de Wal et al., 2002; Divine et al., 2011). The proportion of ice lenses which indicate periods of near zero ice surface temperatures increased from 33 % during the Little Ice Age to 55 % in the 20th century, Pohjola et al. (2002). The surface temperatures have been kept fixed to the observations of the weather stations as stated earlier.

We assume that the penetration depth increases linearly from 0 m at the elevation of an average firn line to a maximum penetration depth at the summit, leading to the effect that firn heating increases with the thickness of the firn layer. This is also in line with the usual approach of calculating refreezing as a fraction of winter accumulation, which is best described on VSF by an elevation gradient (Möller et al., 2011). This is a simplification since in reality the melting should be largest at low (warmer) elevation even though the firn thickness increases with altitude, an effect which is at least partially counterbalanced by the formation of ice lenses, more effectively with more melt, which inhibits penetration of melt water.

The mean elevation of the firn line was digitized from several satellite pictures: Landsat July 1976, September 1988 and August 2006; Spot July 1991 and August 2008; Aster August 2000 and July 2005. Two of these lines (August 2008 and September 1988) have been excluded since the firn lines are located at exceptionally low elevations probably due to abnormally early fresh snow. We observe little change over recent decades, as found by Möller et al. (2013). Since the firn line elevation is approximately uniform over most of the ice cap, a single mean elevation for the firn line is assumed ignoring any other spatial variations. We estimate this mean elevation to be 410 m a.s.l. This is consistent with estimates of the average equilibrium line elevation (326 m a.s.l., Möller et al., 2013), since on Svalbard glaciers the equilibrium line is typically located significantly lower due to extensive superimposed ice formation (Möller et al., 2011; van Pelt et al., 2012). For future prognostics with climatically varying sur-

Heat production sources and dynamics of VSF

M. Schäfer et al.

Title Page

Abstract

Introduction

Conclusions

References

Tables

Figures

⏪

⏩

◀

▶

Back

Close

Full Screen / Esc

Printer-friendly Version

Interactive Discussion



face mass balance the firn line elevation could be parametrized by the elevation of the equilibrium line.

A first run of the model to equilibrium temperature using a maximum penetration depth of 13.5 m leads to a good match with the measurements in the lower part of the drilling hole, see Fig. 7 (blue line). A prognostic run over 30 yr with an increased penetration depth of 18 m starting from this equilibrium state allows then to reproduce fairly well the observed peak in the upper layers (black line). The horizontal distribution of the modeled temperature including firn heating is shown in Fig. 5 and the vertical in Fig. 6.

4.3 Prognostic simulations over the period 1995–2008

To study the evolution of the temperature field we conduct prognostic simulations with three different temporal evolutions of β prescribed and analyze the connected evolution of all system variables. The three simulations are run with full thermomechanical coupling starting from the relaxed 1990 DEM, using present day surface mass balance (Möller et al., 2011) as a forcing. Temperature is initialized to the 1995 steady-state temperature profile. The three basal drag scenarios are:

1. The basal drag coefficient kept constant at the 1995 pattern.
2. A sudden switch after five years to the 2008 pattern (which differs from the 1995 pattern mainly by the acceleration of Franklinbreen).
3. A locally linear change from the 1995 to 2008 values.

All simulations span 1995–2008. Each simulation was run twice – excluding and including firn heating to assess its possible impacts and to detect possible bias due to errors in the firn heating parametrization. Changes in surface elevation and basal temperatures are shown in Figs. 8 and 9.

Title Page

Abstract

Introduction

Conclusions

References

Tables

Figures



Back

Close

Full Screen / Esc

Printer-friendly Version

Interactive Discussion



5 Discussion

5.1 Implications of inferred basal drag coefficient distributions

The basal drag coefficient β is a crucial parameter in simulating the thermodynamical regime of VSF as it is a key control on sliding velocities, which govern both friction heating and heat advection. As shown in Sect. 4.1.1, use of an inverse method to derive the spatially varying basal drag coefficient is largely unaffected by temperature distribution. Conversely, the temperature evolution shows high sensitivity to such an inversion. Surface relaxation (Sect. 4.1.2) reduces this sensitivity by producing smoother velocity fields.

Variations in the basal drag coefficient distribution across the three periods (Fig. 2) connected to large variations in surface velocities and indicate the importance of a time evolving basal drag based on the underlying physical processes. When comparing the obtained basal patterns from 1995, 2008 and 2011, the internal structure of some of the outlet glaciers is slightly different, but the most striking change remains the acceleration of Franklinbreen from 1995 to 2008 featured by a strong increase in basal sliding. The 2011 β -distribution mainly reflects the different changes in velocity pattern in the two branches of Franklinbreen: the northern one is decelerating while the southern one continues to accelerate. Minor changes in the two most eastern outlet glaciers between 2008 and 2011 are more likely artifacts of the data imperfections in the 2008 and 2011 velocity data sets than features of the real system. In all outlet glaciers a distinct spatial variation of β can be seen, indicating that a sliding law also needs to reproduce these variations, especially since Schäfer et al. (2012) have shown that spatially constant sliding coefficients specific to each outlet glacier do not allow reproduction of the observed velocity structure within the outlet glaciers.

TCD

7, 5097–5145, 2013

Heat production sources and dynamics of VSF

M. Schäfer et al.

Title Page

Abstract

Introduction

Conclusions

References

Tables

Figures

◀

▶

◀

▶

Back

Close

Full Screen / Esc

Printer-friendly Version

Interactive Discussion



5.2 Interpretation of a temperature profile from deep drilling

As shown in our simulations in which firn heating is represented (Sect. 4.2), the observed shape of the temperature profile measured in the Motoyama et al. (2008) ice core (Fig. 7) cannot be explained by an equilibrium temperature profile. Our model-supported interpretation requires a recent perturbation away from an earlier equilibrium state, caused by a change in the surface conditions. Van de Wal et al. (2002) came to a similar conclusion when reconstructing the temperature record in the Lomonosovfonna plateau (northeast of Billefjorden/Isfjorden, Spitzbergen). However, they kept the surface temperature as tuning parameter. Their obtained surface temperature is too high and induces a shift of a few Kelvin. Hence model and data fit well in the lower part, but the surface values are unrealistically warm. They conclude a change in surface conditions in the 1920ies from their model and find confirmation for this by comparing to the mean air temperature record at Svalbard airport starting in 1910.

Discrepancy between our model-implied change in the 60s and the actual climatic record can be explained by various reasons: first, as stated earlier, the uncertainty in the basal drag coefficient strongly impacts the evolution of the temperature distribution through advection. Second, only one data set of deep borehole temperatures is available for model calibration. Lastly, our approach might be too simplistic, especially with respect to the assumptions of spatial or elevation dependencies, and the use of penetration depth as the only calibration parameter (surface temperature variations also lead to temperature variations at depth but with different timescales to the penetration depth).

The calibrated penetration depth (13.5 m and 18 m, Sect. 4.2) is deeper than might be expected, since measured relative densities (Motoyama et al., 2008) reach values over 0.85 at 10 m depth and below, i.e. values of ice or ice lenses with very slow percolation. These unrealistically high values for the penetration depth can be explained by the omission of firn layer compressibility in the mechanical model (Zwinger et al.,

TCD

7, 5097–5145, 2013

Heat production sources and dynamics of VSF

M. Schäfer et al.

Title Page

Abstract

Introduction

Conclusions

References

Tables

Figures

◀

▶

◀

▶

Back

Close

Full Screen / Esc

Printer-friendly Version

Interactive Discussion



2007), and imply that our approach should be considered as qualitative rather than quantitative.

With respect to this more recent change in the conditions on the surface, our model predicts that this signal will take over 100 yr to reach the base. Thus for studying basal processes, even for prognostic simulations on a century scale, we can neglect the effects of this change in firn heating (see also Fig. 7). Conversion of the latent energy released at the location of the ice core corresponds at the location of the drilling hole to a P_{\max} value of 0.9, which is in the expected range (Wright, 2005), increasing confidence in our model.

A discrepancy between our equilibrium profile and the data is also apparent in the middle of the depth profile. We explain this either by the fact that the ice cap has not yet reached thermal equilibrium (see the 50/100/150 yr etc. graphs in Fig. 7 for the shape of such profiles in the lower and middle part) or by the impacts of uncertainties in advection (Sect. 5.1).

With our simplified parametrization of latent heat release due to refreezing we are qualitatively able to reproduce the observed profile, indicating that we identified the driving mechanisms behind the measured distribution. Different limitations of this model for a better interpretation of quantitative results have been highlighted. However, in view of the relative robustness to temperature variations of the inverse method (Schäfer et al., 2012) we are confident that the remaining uncertainties or imperfections of our approach are justified in terms of the inversion for the basal drag coefficient and results with respect to the respective roles of the different heat sources.

5.3 The role of heat sources for VSF fast flowing outlet glaciers

A comparison between surface and sliding velocities at the bedrock clearly shows that sliding dominates the ice dynamics at the fast flow areas of VSF, which even holds for increased deformation in the case of by temperature lowered viscosity (Schäfer et al., 2012). Schäfer et al. (2012) further showed that the temperature distribution has little impact on both surface velocities and basal drag coefficient obtained with the inverse

TCD

7, 5097–5145, 2013

Heat production sources and dynamics of VSF

M. Schäfer et al.

Title Page

Abstract

Introduction

Conclusions

References

Tables

Figures

⏪

⏩

◀

▶

Back

Close

Full Screen / Esc

Printer-friendly Version

Interactive Discussion



method. Therefore we focus on the impact of temperature and the respective heat sources on the onset and maintenance of fast flow.

5.3.1 Friction and strain heating

Our results regarding the importance of friction heating are similar to those of Brinkerhoff et al. (2011) for some Greenland outlet glaciers. In the fast outlet glaciers, where basal sliding is important, friction heating is a dominant heat source and is needed to maintain temperate conditions at the bed (Fig. 5). In contrast to Pohjola and Hedfors (2003), who investigated fast flow in Antarctica using a one-dimensional numerical thermodynamic model, the contribution of strain heating is found to be very small on VSF. Strain heat integrated over the whole ice column is at least an order of magnitude lower than friction heat at the bed. Strain heat is mainly confined to the shear margins while friction heat is present over the whole bedrock area of the outlet glaciers. Larour et al. (2012) observed a similar spatial distribution of strain and friction heat, however they find similar magnitudes for both heat sources.

The pattern of simulated friction heating is consistent with the fast flow and sliding areas, except for some of the southern facing outlet glaciers which appear in our results to be cold-based yet fast flowing. Brinkerhoff et al. (2011) discussed the possibility of cold based sliding or underestimation of ice deformation due to neglecting ice anisotropy. Here, cold based sliding occurs mainly in areas where the bedrock elevation is poorly known, so that uncertainties in the ice thickness are certainly the main factor to explain why basal ice does not reach the pressure melting point. Irregularities in the bedrock data and analysis of the 1995–2008 prognostic simulations (Sect. 5.4) confirm this; improvement of the bedrock data by some control method should be considered as for example done by Morlighem et al. (2013) or van Pelt et al. (2013).

Even though this clear correlation between friction heat and sliding was identified, the question how this fast flow was initiated remains open. A possible explanation for the cyclicity of accelerations and decelerations could be a combined thickness – temperature – heat sources feedback: Franklinbreen was in 1990 the thickest of the

Heat production sources and dynamics of VSF

M. Schäfer et al.

Title Page

Abstract

Introduction

Conclusions

References

Tables

Figures



Back

Close

Full Screen / Esc

Printer-friendly Version

Interactive Discussion



Heat production sources and dynamics of VSF

M. Schäfer et al.

Title Page

Abstract

Introduction

Conclusions

References

Tables

Figures

◀

▶

◀

▶

Back

Close

Full Screen / Esc

Printer-friendly Version

Interactive Discussion



outlet glaciers and the only outlet glacier featuring some areas with sub-melt sliding (Hindmarsh and Meur, 2001), even in the absence of additional heat sources. By its reduced ice velocities it might have thickened enough to allow basal ice to approach pressure melting point through insulation and in turn triggering sliding. Thickening of Franklinbreen especially in the lower part between 1990 and 2005 is confirmed by Nuth et al. (2010). Various temperature feedbacks like the one involving friction heating could then have reinforced and maintained this acceleration. However, no complete surface DEMs from different periods are available. Neither Nuth et al. (2010) nor Moholdt et al. (2010) observed a thinning on Franklinbreen between 1990–2005 or between 2003–2008. Even though Nuth et al. (2010) observe large errors over Franklinbreen (average $0.06 \pm 0.12 \text{ myr}^{-1}$) it seems unlikely that the recent reduction of the acceleration visible from comparing the 2008 and similar 2011 velocities on Franklinbreen is driven simply by a negative feedback involving thinning.

5.3.2 Firn heating due to melt water refreezing

Firn heating is important for the general thermal regime of the ice cap and can have larger impacts than friction or strain heating in some regions (Figs. 5 and 6). Our model shows an increase in basal temperature in the onset area of Franklinbreen due to firn heating (Fig. 5). However, since similar increases occur at non-accelerating glaciers, we rule this out as the sole trigger for speed-ups of outlet glaciers. It would still have an impact on the basal sliding of already fast flowing glaciers. The temperature signal of a recent increase in latent heat release cannot possibly have reached the bedrock to explain the recent acceleration (Fig. 7). Also because of the long diffusive time scale (centuries) for temperature (Fig. 7) we do not expect firn heating to be the maintaining mechanism behind a lasting acceleration. Nevertheless it could be possible that firn heating has indirect impacts affecting the englacial hydrology.

5.4 Evolution of the temperature field in prognostic runs

Focusing on Franklinbreen, as expected in scenario (1) (see Sect. 4.3) the velocity pattern remains constant. In scenario (2) a sudden increase in velocities after the change in basal drag coefficient is followed by a small deceleration. In scenario (3) the velocities increase synchronous with changes in basal drag coefficient (Fig. 2). The 2008 velocities are identical in scenarios (2) and (3). Scenarios (2) and (3) exhibit a clear thinning of the onset area of Franklinbreen relative to (1) (Fig. 8). This is more pronounced (up to 25 m compared to 20 m) in scenario (2) resulting from the time integrated ice flux which is higher the sooner the velocities increase. The pronounced increase in thickness at the terminus of Franklinbreen can be interpreted as a model feature caused by fixing geometry horizontally and neglecting calving. Other outlet glaciers, especially Rijpbreen and Bodlebreen, are highly influenced by errors in the bedrock DEM and thus not discussed.

Temperature remains unchanged in scenario (1). In scenarios (2) and (3) however, the model shows a warming of around 2 K at Franklinbreen's lateral margins. Temperature changes are not restricted to ice at the bed. An approach to designing a physically based sliding law would be to allow sliding where temperature approaches pressure melting point. The area in which this occurs increases slightly in both scenarios. In scenario (2), the temperature adjusts smoothly during the years following the jump to a similar pattern as in scenario (3); no sudden jump in basal temperature is visible in spite of the step change in basal drag coefficient. The friction heat production changes in the same way in scenarios (2) and (3) over Franklinbreen and its onset area, reaching fairly high up to the center of the ice cap. Similarly strain heat increases in both scenarios at the lateral margins of Franklinbreen and over the whole ice column. In scenario (2), both heat sources undergo a sudden jump synchronous with the jump in basal friction parameter. No striking spatial correlation between the basal drag coefficient and friction heat is apparent; friction heating is important where velocities are

TCD

7, 5097–5145, 2013

Heat production sources and dynamics of VSF

M. Schäfer et al.

Title Page

Abstract

Introduction

Conclusions

References

Tables

Figures

◀

▶

◀

▶

Back

Close

Full Screen / Esc

Printer-friendly Version

Interactive Discussion



plemented by Seddik et al. (2012) and Dunse et al. (2011), only the change in the area of temperatures close to pressure melting point can be responsible for acceleration/deceleration processes. Since these changes are rather small, this seems unlikely. Also, such parametrization is not based on physical mechanisms and would require good knowledge of the temperature distribution at least as initial condition which is highly uncertain for ice caps like VSF. Since the whole area at the bedrock of the outlet glaciers is at the same temperature, a sliding law depending only on temperature would not allow for the fine structure in the basal drag coefficient needed to reproduce the correct velocity structure inside the outlet glaciers (Schäfer et al., 2012). Accounting for either equilibrium or transient impact of firn heating does not alter these results (Fig. 9).

6 Conclusions

In this work we present the basal drag coefficient distribution obtained on the VSF ice cap at different periods. A clear acceleration between 1995 and 2008 on one of the outlet glaciers (Franklinbreen) is observed and reflected in a pronounced temporal variation of the distribution of the basal drag coefficient. Since the change from 1995 to 2008 is significant for future simulations, a sliding law incorporating mechanisms governing acceleration and deceleration of outlet glaciers would be needed in order to conduct reliable future simulations for ice caps like VSF.

Friction heating is identified as a key factor for maintaining warm basal conditions, however no concrete feedback or mechanism for the onset of the acceleration of Franklinbreen has yet been identified. Strain heating is negligible compared to friction heating and important only in the shear-margins.

The temperature profile measured in a deep borehole in the accumulation zone has been successfully modeled and qualitatively explained. Uncertainties in the basal drag coefficient distribution and its consequences for advection have been identified as one of the limiting factors for qualitative interpretations of results of our firn heating

Heat production sources and dynamics of VSF

M. Schäfer et al.

Title Page

Abstract

Introduction

Conclusions

References

Tables

Figures



Back

Close

Full Screen / Esc

Printer-friendly Version

Interactive Discussion



Heat production sources and dynamics of VSF

M. Schäfer et al.

Title Page

Abstract

Introduction

Conclusions

References

Tables

Figures

◀

▶

◀

▶

Back

Close

Full Screen / Esc

Printer-friendly Version

Interactive Discussion



parametrization. Recent deviations from an equilibrium profile triggered by increased firn heating can explain the current shape of the profile and additionally could be a trigger for speed-ups, but cannot be the main driver of fast flow. Timescales of temperature changes induced by changing surface conditions to reach the bottom in the simulations including firn heating are estimated at several centuries.

Velocities and heat sources adjust instantaneously to changes in basal drag while temperature adjusts to changes on a time scale of years to decades in the central areas. However we are fairly confident that in fast flowing areas the assumption of steady-state temperature profiles is justified, while further inland in the slow central areas longer times might be needed for adjustment.

From our prognostic simulations between 1995 and 2008, we conclude that the acceleration is clearly reflected in the basal pattern, but cannot be explained by the temperature distribution as the only parameter, even though part of such direct link between temperature and basal drag could be obscured through our assumption of steady-state temperature. We conclude that the fast flow is not solely linked to temperature, but also to basal hydrology and sediment processes, even though various temperature dependent feedbacks do play an important role.

Appendix A

Forward diagnostic model

The forward ice flow model is described in more detail by Schäfer et al. (2012); Gagliardini et al. (2013). The ice is considered as non-linear viscous incompressible material flowing under gravity over a rigid bedrock. The mass conservation equation reduces because of incomprehensibility to

$$\frac{\partial v_x}{\partial x} + \frac{\partial v_y}{\partial y} + \frac{\partial v_z}{\partial z} = 0, \quad (\text{A1})$$

where v_x, v_y, v_z denote the components along the three directions of space of the velocity vector \mathbf{v} . Applying Einstein's convention for summation of same indexes, the stress tensor $\boldsymbol{\tau}$ splits into a deviatoric part $\boldsymbol{\tau}'$ and the isotropic pressure p

$$\tau_{ij} = \tau'_{ij} - p\delta_{ij}, \quad (\text{A2})$$

5 where index notation is used and δ_{ij} is the Kronecker symbol. The second invariant τ_* of the deviatoric stress tensor is defined as

$$\tau_*^2 = \frac{1}{2} \tau'_{ij} \tau'_{ij}. \quad (\text{A3})$$

The deviatoric stress components are linked to the strain rates $\dot{\epsilon}$ through the constitutive relation, which is a power law, referred to as the Glen's flow law in glaciology

$$10 \quad \dot{\epsilon}_{ij} = A(T) \tau_*^2 \tau'_{ij}, \quad (\text{A4})$$

with $A(T)$ the deformation rate factor. The strain rate components, $\dot{\epsilon}_{ij}$, are defined from the velocity components as

$$\dot{\epsilon}_{ij} = \frac{1}{2} \left(\frac{\partial v_i}{\partial x_j} + \frac{\partial v_j}{\partial x_i} \right), \quad i, j = x, y, z. \quad (\text{A5})$$

15 The force balance (quasi static equilibrium) in the three directions of space leads to the Stokes equations

$$\begin{aligned} \frac{\partial \sigma_x}{\partial x} + \frac{\partial \tau_{xy}}{\partial y} + \frac{\partial \tau_{xz}}{\partial z} &= 0, \\ \frac{\partial \tau_{xy}}{\partial x} + \frac{\partial \sigma_y}{\partial y} + \frac{\partial \tau_{yz}}{\partial z} &= 0, \\ \frac{\partial \tau_{xz}}{\partial x} + \frac{\partial \tau_{yz}}{\partial y} + \frac{\partial \sigma_z}{\partial z} &= \rho g, \end{aligned} \quad (\text{A6})$$

Heat production sources and dynamics of VSF

M. Schäfer et al.

Title Page

Abstract

Introduction

Conclusions

References

Tables

Figures

◀

▶

◀

▶

Back

Close

Full Screen / Esc

Printer-friendly Version

Interactive Discussion



where σ_i stands for τ_{ij} , $g = 9.81 \text{ m s}^{-2}$ is the norm of the gravitational acceleration vector \mathbf{g} , and $\rho = 910 \text{ kg m}^{-3}$ is the glacier ice density.

Authors' contribution

M. Schäfer designed and conducted the simulations, F. Gillet-Chaulet implemented the inverse method, R. Gladstone contributed to experimental setup, R. Pettersson and V. A. Pohjola provided data, T. Strozzi provided the remote sensing data of the surface velocities, T. Zwinger helped with the numerical setup. All authors have contributed to, seen and approved the manuscript.

Acknowledgements. We would like to thank all partners for access to data and constructive comments, we would like to mention especially the German and Norwegian teams for access to their AWS data (Roman Finkelnburg, Marco Möller, Dieter Scherer, Christoph Schneider, Thomas Vikhamar Schuler and others) as well as Björn Claremar and Jon Jörpeland for discussion about their results from WRF simulations. We acknowledge CSC – IT Center for Science Ltd. for the allocation of computational resources. The velocity data were produced with support of the EU FP6 INTEGRAL Project (1995), the ESA DUE GLOBGLACIER Project (2008) and the EU FP7 CRYOLAND Project (2011). We also would like to thank Ilmo Kukkonen for valuable discussions on the geological background. This work was performed at the Arctic Centre at the University of Lapland through funding of the Finnish Academy, the projects SvalGlac and SVALI. R. Pettersson and V. A. Pohjola were funded by the Swedish Science Council. This publication is contribution number 25 of the Nordic Centre of Excellence SVALI, Stability and Variations of Arctic land Ice, funded by the Nordic Top-level Research Initiative.

References

- Arthern, R. J. and Gudmundsson, G. H.: Initialization of ice-sheet forecasts viewed as an inverse Robin problem, *J. Glaciol.*, 56, 527–533, 2010. 5109
- Bougamont, M., Price, S., Christoffersen, P., and Payne, A. J.: Dynamic patterns of ice stream flow in a 3D higher-order ice sheet model with plastic bed and simplified hydrology, *J. Geophys. Res.*, 116, F04018, doi:10.1029/2011JF002025, 2011. 5100

Heat production sources and dynamics of VSF

M. Schäfer et al.

Title Page

Abstract

Introduction

Conclusions

References

Tables

Figures

◀

▶

◀

▶

Back

Close

Full Screen / Esc

Printer-friendly Version

Interactive Discussion



Heat production sources and dynamics of VSF

M. Schäfer et al.

Title Page

Abstract

Introduction

Conclusions

References

Tables

Figures

◀

▶

◀

▶

Back

Close

Full Screen / Esc

Printer-friendly Version

Interactive Discussion



- Boulton, G. S. and Jones, A. S.: Stability of temperate ice caps and ice sheets resting on beds of deformable sediment, *J. Glaciol.*, 24, 29–43, 1979. 5099
- Braun, M., Pohjola, V. A., Pettersson, R., Möller, M., Finkelnburg, R., Falk, U., Scherer, D., and Schneider, C.: Changes of glacier frontal positions of Vestfonna (Nordaustlandet, Svalbard), *Geogr. Ann. A*, 93, 301–310, doi:10.1111/j.1468-0459.2011.00437.x, 2011. 5102
- Brinkerhoff, D. J., Meierbachtol, T. W., Johnson, J. V., and Harper, J. T.: Sensitivity of the frozen/melted basal boundary to perturbations of basal traction and geothermal heat flux: Isunnguata Sermia, western Greenland, *Ann. Glaciol.*, 52, 43–50, 2011. 5121
- Clarke, G. K. C., Nitsan, U., and Paterson, W. S. B.: Flow-switching and water piracy between Rutford Ice Stream and Carlson Inlet, West Antarctica, *Rev. Geophys.*, 15, 235–247, 1977. 5100
- Divine, D., Isaksson, E., Martma, T., Meijer, H., Moore, J., Pohjola, V., van de Wal, R., and Godtliobsen, F.: Thousand years of winter surface air temperature variations in Svalbard and northern Norway reconstructed from ice core data, *Polar Res.*, 30, 7379, doi:10.3402/polar.v30i0.7379, 2011. 5116
- Dowdeswell, J. A., Benham, T. J., Strozzi, T., and Hagen, J. O.: Iceberg calving flux and mass balance of the Austfonna ice cap on Nordaustlandet, Svalbard, *J. Geophys. Res.-Earth*, 113, F03022, doi:10.1029/2007JF000905, 2008. 5103
- Dunse, T., Greve, R., Schuler, T. V., and Hagen, J. O.: Permanent fast flow vs. cyclic surge behaviour: numerical simulations of the Austfonna ice cap, Svalbard, *J. Glaciol.*, 57, 247–259, 2011. 5125
- Dunse, T., Schuler, T. V., Hagen, J. O., and Reijmer, C. H.: Seasonal speed-up of two outlet glaciers of Austfonna, Svalbard, inferred from continuous GPS measurements, *The Cryosphere*, 6, 453–466, doi:10.5194/tc-6-453-2012, 2012. 5099
- Fowler, A., Murray, T., and Ng, F.: Thermally controlled glacier surging, *J. Glaciol.*, 47, 527–538, doi:10.3189/172756501781831792, 2001. 5100
- Fowler, A. C., Toja, R., and Vazquez, C.: Temperature-dependent shear flow and the absence of thermal runaway in valley glaciers, *Proc. R. Soc. A*, 466, 363–382, doi:10.1098/rspa.2009.0335, 2010. 5100
- Frey, P. J.: YAMS: A fully automatic adaptive isotropic surface remeshing procedure, Rapport technique, INRIA, 0252, 2001. 5110

Heat production sources and dynamics of VSF

M. Schäfer et al.

Title Page

Abstract

Introduction

Conclusions

References

Tables

Figures

◀

▶

◀

▶

Back

Close

Full Screen / Esc

Printer-friendly Version

Interactive Discussion



Gagliardini, O. and Zwinger, T.: The ISMIP-HOM benchmark experiments performed using the Finite-Element code Elmer, *The Cryosphere*, 2, 67–76, doi:10.5194/tc-2-67-2008, 2008. 5105

5 Gagliardini, O., Zwinger, T., Gillet-Chaulet, F., Durand, G., Favier, L., de Fleurian, B., Greve, R., Malinen, M., Martín, C., Råback, P., Ruokolainen, J., Sacchetti, M., Schäfer, M., Seddik, H., and Thies, J.: Capabilities and performance of Elmer/Ice, a new-generation ice sheet model, *Geosci. Model Dev.*, 6, 1299–1318, doi:10.5194/gmd-6-1299-2013, 2013. 5105, 5110, 5126

10 Gillet-Chaulet, F., Gagliardini, O., Seddik, H., Nodet, M., Durand, G., Ritz, C., Zwinger, T., Greve, R., and Vaughan, D. G.: Greenland ice sheet contribution to sea-level rise from a new-generation ice-sheet model, *The Cryosphere*, 6, 1561–1576, doi:10.5194/tc-6-1561-2012, 2012. 5109, 5110

Greve, R.: Application of a polythermal three-dimensional ice sheet model to the Greenland ice sheet: response to steady-state and transient climate scenarios, *J. Climate*, 10, 901–918, 1997. 5101

15 Greve, R. and Blatter, H.: Dynamics of ice sheets and glaciers, in: *Advances in Geophysics and Environmental Mechanics and Mathematics*, Springer Dordrecht Heidelberg London New York, 2009. 5106

Habermann, M., Maxwell, D., and Truffer, M.: Reconstruction of basal properties in ice sheets using iterative inverse methods, *J. Glaciol.*, 58, 795–807, doi:10.3189/2012JoG11J168, 2012. 5101, 5109

20 Hagen, J. O., Liestol, O., Roland, E., and Jorgensen, T.: *Glacier atlas of Svalbard and Jan Mayen*, Norsk Polar Institut, Oslo, 1993. 5104

Hansen, P.: The L-curve and its use in the numerical treatment of inverse problems, *Computational inverse problems in electrocardiology*, 5, 119–142, 2001. 5112

25 Hindmarsh, R. C. A.: Consistent generation of ice-streams via thermo-viscous instabilities modulated by membrane stresses, *Geophys. Res. Lett.*, 36, L06502, doi:10.1029/2008GL036877, 2009. 5100

Hindmarsh, R. C. and Meur, E. L.: Dynamical processes involved in the retreat of marine ice sheets, *J. Glaciol.*, 47, 271–282, doi:10.3189/172756501781832269, 2001. 5122, 5124

30 Hines, K. M., Bromwich, D. H., Bai, L.-S., Barlage, M., and Slater, A. G.: Development and testing of Polar WRF, Part III: Arctic land, *J. Climate*, 24, 26–48, doi:10.1175/2010JCLI3460.1, 2011. 5104

Heat production sources and dynamics of VSF

M. Schäfer et al.

Title Page

Abstract

Introduction

Conclusions

References

Tables

Figures

◀

▶

◀

▶

Back

Close

Full Screen / Esc

Printer-friendly Version

Interactive Discussion



Ignatieva, I. and Macheret, Y.: Evolution of Nordaustlandet ice caps in Svalbard under climate warming, IAHS Publ. 208 (Symposium at St. Petersburg 1990 – Glaciers–Ocean – Atmosphere Interactions), 301–312, 1991. 5105

Iken, A.: The effect of subglacial water pressure on the sliding velocity of a glacier in an idealized numerical model, *J. Glaciol.*, 27, 407–422, 1981. 5099

Jacob, T., Wahr, J., Pfeffer, W. T., and Swenson, S.: Recent contributions of glaciers and ice caps to sea level rise, *Nature*, 482, 514–518, doi:10.1038/nature10847, 2012. 5099

Jakobsson, M., Macnab, R., Mayer, M., Anderson, R., Hatzky, M. E. J., Schenke, H.-W., and Johnson, P.: An improved bathymetric portrayal of the Arctic Ocean: Implications for ocean modeling and geological, geophysical and oceanographic analyses, *Geophys. Res. Lett.*, 35, L07602, doi:10.1029/2008GL033520, 2008. 5102

Jay-Allemand, M., Gillet-Chaulet, F., Gagliardini, O., and Nodet, M.: Investigating changes in basal conditions of Variegated Glacier prior to and during its 1982–1983 surge, *The Cryosphere*, 5, 659–672, doi:10.5194/tc-5-659-2011, 2011. 5101, 5109

Kamb, B.: Glacier surge mechanism based on linked cavity configuration of the basal water conduit system, *J. Geophys. Res.*, 92, 9083–9100, doi:10.1029/JB092iB09p09083, 1987. 5100

Kamb, B.: Basal zone of the West Antarctic Ice Streams and its role in lubrication of their rapid motion, *Antarct. Res. Ser.*, 77, 157–199, doi:10.1029/AR077p0157, 2001. 5100

Larour, E., Morlighem, M., Seroussi, H., Schiermeier, J., and Rignot, E.: Ice flow sensitivity to geothermal heat flux of Pine Island Glacier, Antarctica, *J. Geophys. Res.-Earth*, 117, F04023, doi:10.1029/2012JF002371, 2012. 5121

Lee, W. H. K.: On the global variations of terrestrial heat-flow, *Phys. Earth Planet. Interiors*, 2, 332–341, 1970. 5105

Liljequist, G.: High Latitudes, The Swedish Polar Research Secretariat/Streiffert, 607 pp., 1993. 5104

Mayo, L. R.: Identification of unstable glaciers intermediate between normal and surging glaciers, Academy of Sciences of the USSR, Section of Glaciology of the Soviet Geophysical Committee and Institute of Geography, Moscow. Data of Glaciological Studies, Publication 33, Proceedings (Alma-Ata, 1976), vol. 47–55, 133–135, 1978. 5099

Meier, M. F., Dyurgerov, M. B., Rick, U. K., O’Neel, S., Pfeffer, W. T., Anderson, R. S., Anderson, S. P., and Glazovsky, A. F.: Glaciers dominate Eustatic sea-level rise in the 21st century, *Science*, 317, 1064–1067, doi:10.1126/science.1143906, 2007. 5099

Heat production sources and dynamics of VSF

M. Schäfer et al.

Title Page

Abstract

Introduction

Conclusions

References

Tables

Figures

◀

▶

◀

▶

Back

Close

Full Screen / Esc

Printer-friendly Version

Interactive Discussion



Moholdt, G., Nuth, C., Hagen, J. O., and Kohler, J.: Recent elevation changes of Svalbard glaciers derived from ICESat laser altimetry, *Remote Sens. Environ.*, 114, 2756–2767, doi:10.1016/j.rse.2010.06.008, 2010. 5113, 5122

Möller, M., Finkelnburg, R., Braun, M., Hock, R., Jonsell, U., Pohjola, V. A., Scherer, D., and Schneider, C.: Climatic mass balance of the ice cap Vestfonna, Svalbard: a spatially distributed assessment using ERA-Interim and MODIS data, *J. Geophys. Res.*, 116, F03009, doi:10.1029/2010JF001905, 2011. 5104, 5116, 5117

Möller, M., Finkelnburg, R., Braun, M., Scherer, D., and Schneider, C.: Variability of the climatic mass balance of Vestfonna ice cap (northeastern Svalbard), 1979–2011, *Ann. Glaciol.*, 54(63), 2013. 5116

Moon, T., Joughin, I., Smith, B., and Howat, I.: 21st-century evolution of Greenland outlet glacier velocities, *Science*, 336, 576–578, doi:10.1126/science.1219985, 2012. 5099

Moore, J. C., Jevrejeva, S., and Grinsted, A.: The historical global sea level budget, *Ann. Glaciol.*, 52, 8–14, 2011. 5099

Morlighem, M., Rignot, E., Seroussi, H., Larour, E., Dhia, H. B., and Aubry, D.: Spatial patterns of basal drag inferred using control methods from a full-Stokes and simpler models for Pine Island Glacier, West Antarctica, *Geophys. Res. Lett.*, 37, L14502, doi:10.1029/2010GL043853, 2010. 5101

Morlighem, M., Rignot, E., Mouginit, J., Wu, X., Seroussi, H., Larour, E., and Paden, J.: High-resolution bed topography mapping of Russell Glacier, Greenland, inferred from Operation IceBridge data, *J. Glaciol.*, 59, in press, doi:10.3189/2013JoG12J235, 2013. 5121

Motoyama, H., Watanabe, O., Fuji, Y., Kamiyama, K., Igarashi, M., Matoba, S., Kameda, T., Goto-Azuma, K., Izumi, K., Narita, H., Iizuka, Y., and Isaksson, E.: Analyses of ice Core Data from Various Sites in Svalbard Glaciers from 1987 to 1999, *NIPR Arctic Data Reports*, 7, 2008. 5105, 5108, 5115, 5119, 5143

Murray, T., Stuart, G., Miller, P., Woodward, J., Smith, A., Porter, P., and Jiskoot, H.: Glacier surge propagation by thermal evolution at the bed, *J. Geophys. Res.-Solid*, 105, 13491–13507, doi:10.1029/2000JB900066, 2000. 5100

Murray, T., Strozz, T., Luckman, A., Jiskoot, H., and Christakos, P.: Is there a single surge mechanism? Contrasts in dynamics between glacier surges in Svalbard and other regions, *J. Geophys. Res.-Solid*, 108, 2237, doi:10.1029/2002JB001906, 2003. 5100

Heat production sources and dynamics of VSF

M. Schäfer et al.

Title Page

Abstract

Introduction

Conclusions

References

Tables

Figures

◀

▶

◀

▶

Back

Close

Full Screen / Esc

Printer-friendly Version

Interactive Discussion



- Nuth, C., Moholdt, G., Kohler, J., Hagen, J. O., and Kaab, A.: Svalbard glacier elevation changes and contribution to sea level rise, *J. Geophys. Res.-Earth*, 115, F01008, doi:10.1029/2008JF001223, 2010. 5113, 5122
- Payne, A. and Dongelmans, P.: Self-organization in the thermomechanical flow of ice sheets, *J. Geophys. Res.-Solid*, 102, 12219–12233, doi:10.1029/97JB00513, 1997. 5100
- Payne, A., Huybrechts, P., Abe-Ouchi, A., Calov, R., Fastook, J., Greve, R., Marshall, S., Marsiat, I., Ritz, C., Tarasov, L., and Thomassen, M.: Results from the EISMINT model intercomparison: the effects of thermomechanical coupling, *J. Glaciol.*, 46, 227–238, doi:10.3189/172756500781832891, 2000. 5100
- Pettersson, R., Christoffersen, P., Dowdeswell, J. A., Pohjola, V. A., Hubbard, A., and Strozzì, T.: Ice thickness and basal conditions of Vestfonna ice cap, Eastern Svalbard, *Geogr. Ann. A*, 93, 311–322, doi:10.1111/j.1468-0459.2011.00438.x, 2011. 5102, 5114
- Pohjola, V. and Hedfors, J.: Studying the effects of strain heating on glacial flow within outlet glaciers from the Heimfrontfjella Range, Dronning Maud Land, Antarctica, *Ann. Glaciol.*, 37, 134–142, doi:10.3189/172756403781815843, International Symposium on Physical and Mechanical Processes on Ice in Relation to Glacier and Ice-Sheet Modelling, Chamonix, FRANCE, 25–30 August 2002, 2003. 5100, 5121
- Pohjola, V., Moore, J., Isaksson, E., Jauhiainen, T., van de Wal, R., Martma, T., Meijer, H., and Vaikmaa, R.: Effect of periodic melting on geochemical and isotopic signals in an ice core from Lomonosovfonna, Svalbard, *J. Geophys. Res.-Atmos.*, 107, 4036, doi:10.1029/2000JD000149, 2002. 5104, 5116
- Pohjola, V. A., Christoffersen, P., Kolondra, L., Moore, J. C., Pettersson, R., Schäfer, M., Strozzì, T., and Reijmer, C. H.: Spatial distribution and change in the surface ice-velocity field of Vestfonna ice cap, Nordaustlandet, Svalbard, 1995–2010 using geodetic and satellite interferometry data, *Geogr. Ann. A*, 93, 323–335, doi:10.1111/j.1468-0459.2011.00441.x, 2011. 5100, 5101, 5102, 5103
- Pralong, M. R. and Gudmundsson, G. H.: Bayesian estimation of basal conditions on Rutford Ice Stream, West Antarctica, from surface data, *J. Glaciol.*, 57, 315–324, 2011. 5101
- Price, S. F., Conway, H., Waddington, E. D., and Bindshadler, R. A.: Model investigations of inland migration of fast-flowing outlet glaciers and ice streams, *J. Glaciol.*, 54, 49–60, doi:10.3189/002214308784409143, 2008. 5100

Heat production sources and dynamics of VSF

M. Schäfer et al.

Title Page

Abstract

Introduction

Conclusions

References

Tables

Figures

◀

▶

◀

▶

Back

Close

Full Screen / Esc

Printer-friendly Version

Interactive Discussion



- Quiquet, A., Ritz, C., Punge, H. J., and Salas y Méliá, D.: Greenland ice sheet contribution to sea level rise during the last interglacial period: a modelling study driven and constrained by ice core data, *Clim. Past*, 9, 353–366, doi:10.5194/cp-9-353-2013, 2013. 5101
- 5 Rignot, E., Velicogna, I., van den Broeke, M. R., Monaghan, A., and Lenaerts, J.: Acceleration of the contribution of the Greenland and Antarctic ice sheets to sea level rise, *Geophys. Res. Lett.*, 38, L05503, doi:10.1029/2011GL046583, 2011. 5099
- Ritz, C., Rommelaere, V., and Dumas, C.: Modeling the evolution of Antarctic ice sheet over the last 420 000 years: implications for altitude changes in the Vostok region, *J. Geophys. Res.-Atmos.*, 106, 31943–31964, doi:10.1029/2001JD900232, 2001. 5101
- 10 Schäfer, M., Zwinger, T., Christoffersen, P., Gillet-Chaulet, F., Laakso, K., Pettersson, R., Pohjola, V. A., Strozzi, T., and Moore, J. C.: Sensitivity of basal conditions in an inverse model: Vestfonna ice cap, Nordaustlandet/Svalbard, *The Cryosphere*, 6, 771–783, doi:10.5194/tc-6-771-2012, 2012. 5101, 5103, 5105, 5107, 5109, 5110, 5112, 5113, 5118, 5120, 5125, 5126, 5142
- 15 Schoof, C.: On the mechanics of ice-stream shear margins, *J. Glaciol.*, 50, 208–218, doi:10.3189/172756504781830024, 2004. 5100
- Schuler, T. V., Loe, E., Taurisano, A., Eiken, T., Hagen, J. O., and Kohler, J.: Calibrating a surface mass balance model for the Austfonna ice cap, Svalbard, *Ann. glaciol.*, 46, 241–248, 2007a. 5104
- 20 Schuler, T. V., Loe, E., Taurisano, A., Eiken, T., Hagen, J. O., and Kohler, J.: Calibrating a surface mass balance model for the Austfonna ice cap, Svalbard, *Ann. Glaciol.*, 46, 241–248, 2007b. 5104
- Schytt, V.: Scientific results of the Swedish glaciological expedition to Nordaustlandet, Spitsbergen, 1957 and 1958, *Geogr. Ann.*, 46, 243–281, 1964. 5102
- 25 Seddik, H., Greve, R., Zwinger, T., Gillet-Chaulet, F., and Gagliardini, O.: Simulations of the Greenland ice sheet 100 years into the future with the full Stokes model Elmer/Ice, *J. Glaciol.*, 58, 427–440, doi:10.3189/2012jog11j177, 2012. 5125
- Seroussi, H., Morlighem, M., Rignot, E., Larour, E., Aubry, D., Dhia, H. B., and Kristensen, S. S.: Ice flux divergence anomalies on 79 north Glacier, Greenland, *Geophys. Res. Lett.*, 38, L09501, doi:10.1029/2011GL047338, 2011. 5112
- 30 Seroussi, H., Morlighem, M., Rignot, E., Khazendar, A., Larour, E., and Mouginot, J.: Dependence of Greenland ice sheet projections on its thermal regime, *J. Glaciol.*, 59, in press, doi:10.3189/2013JoG13J054, 2013. 5112

**Heat production
sources and
dynamics of VSF**

M. Schäfer et al.

Title Page

Abstract

Introduction

Conclusions

References

Tables

Figures

◀

▶

◀

▶

Back

Close

Full Screen / Esc

Printer-friendly Version

Interactive Discussion



- Shepherd, A., Ivins, E. R., Geruo, A., Barletta, V. R., Bentley, M. J., Bettadpur, S., Briggs, K. H., Bromwich, D. H., Forsberg, R., Galin, N., Horwath, M., Jacobs, S., Joughin, I., King, M. A., Lenaerts, J. T. M., Li, J., Ligtenberg, S. R. M., Luckman, A., Luthcke, S. B., McMillan, M., Meister, R., Milne, G., Mouginit, J., Muir, A., Nicolas, J. P., Paden, J., Payne, A. J., Pritchard, H., Rignot, E., Rott, H., Sorensen, L. S., Scambos, T. A., Scheuchl, B., Schrama, E. J. O., Smith, B., Sundal, A. V., van Angelen, J. H., van de Berg, W. J., van den Broeke, M. R., Vaughan, D. G., Velicogna, I., Wahr, J., Whitehouse, P. L., Wingham, D. J., Yi, D., Young, D., and Zwally, H. J.: A reconciled estimate of ice-sheet mass balance, *Science*, 338, 1183–1189, doi:10.1126/science.1228102, 2012. 5099
- Skamarock, W., Klemp, J., Dudhia, J., Gill, D., Barker, D., Duda, M., Yu Huang, X., and Wang, W.: A description of the advanced research WRF version 3, NCAR Technical Note, doi:10.5065/D68S4MVH, 2008. 5104
- Sund, M., Eiken, T., Hagen, J., and Kääb, A.: Svalbard surge dynamics derived from geometric changes., *Ann. Glaciol.*, 50, 50–60, 2009. 5100
- Sund, M., Eiken T., Schneevoigt, T., and Hagen, J.: Towards a revised and synthesized conceptual surge model, in: *On the Dynamics of Surge-Type and Tidewater Glaciers in Svalbard*, PhD thesis, Faculty of Mathematics and Natural Sciences, University of Oslo, Oslo, ISSN 1501-7710, No. 1147, 2011. 5100
- Tidewater Glacier Workshop Report: Baeseman, J. and Early Career Scientists (Workshop participants), IASC report, in: *Report from the Field Workshop on Studies of Tidewater Glaciers*, edited by: Jania, J. A. and Szafraniec, J., Polish Polar Consortium, Faculty of Earth Sciences, University of Silesia, Sosnowiec, Poland, ISBN: 978-3-9813637-5-3, 2013. 5099
- Truffer, M., Harrison, W., and Echelmeyer, K.: Glacier motion dominated by processes deep in underlying till, *J. Glaciol.*, 46, 213–221, doi:10.3189/172756500781832909, 2000. 5100
- Van de Wal, R., Mulvaney, R., Isaksson, E., Moore, J., Pinglot, J., Pohjola, V., and Thomassen, P.: Reconstruction of the historical temperature trend from measurements in a medium-length borehole on the Lomonosovfonna plateau, Svalbard, *Ann. Glaciol.*, 35, 371–378, doi:10.3189/172756402781816979, International Symposium on Ice Cores and Climate, Kangerlussuaq, Greenland, 19–23 August 2001, 2002. 5116, 5119
- van der Wel, N., Christoffersen, P., and Bougamont, M.: The influence of subglacial hydrology on the flow of Kamb Ice Stream, West Antarctica, *J. Geophys. Res.-Earth*, 118, 97–110, doi:10.1029/2012JF002570, 2013. 5100

Heat production sources and dynamics of VSF

M. Schäfer et al.

Title Page

Abstract

Introduction

Conclusions

References

Tables

Figures

◀

▶

◀

▶

Back

Close

Full Screen / Esc

Printer-friendly Version

Interactive Discussion



- Van Pelt, W. J. J. and Oerlemans, J.: Numerical simulations of cyclic behaviour in the Parallel Ice Sheet Model (PISM), *J. Glaciol.*, 58, 347–360, doi:10.3189/2012JoG11J217, 2012. 5100
- van Pelt, W. J. J., Oerlemans, J., Reijmer, C. H., Pohjola, V. A., Pettersson, R., and van Angelen, J. H.: Simulating melt, runoff and refreezing on Nordenskiöldbreen, Svalbard, using a coupled snow and energy balance model, *The Cryosphere*, 6, 641–659, doi:10.5194/tc-6-641-2012, 2012. 5116
- van Pelt, W. J. J., Oerlemans, J., Reijmer, C. H., Pettersson, R., Pohjola, V. A., Isaksson, E., and Divine, D.: An iterative inverse method to estimate basal topography and initialize ice flow models, *The Cryosphere*, 7, 987–1006, doi:10.5194/tc-7-987-2013, 2013. 5121
- Vaughan, D. G., Corr, H. F. J., Smith, A. M., Pritchard, H. D., and Shepherd, A.: Flow-switching and water piracy between Rutford Ice Stream and Carlson Inlet, West Antarctica, *J. Glaciol.*, 54, 41–48, doi:10.3189/002214308784409125, 2008. 5100
- Wadham, J. and Nuttall, A. M.: Multiphase formation of superimposed ice during a mass-balance year at a maritime high-Arctic glaciers, *J. Glaciol.*, 48, 545–551, 2002. 5104
- Wadham, J., Kohler, J., Hubbard, A., Nuttall, A. M., and Rippin, D.: Superimposed ice regime of a high Arctic glacier inferred using ground-penetrating radar, flow modeling, and ice cores, *J. Geophys. Res.*, 111, F01007, doi:10.1029/2004JF000144, 2006. 5104
- Wright, A. P.: The impact of meltwater refreezing on the mass balance of a high Arctic glacier, PhD thesis, University Bristol, 2005. 5120
- Wright, A. P., Wadham, J. L., Siegert, M. J., Luckman, A., Kohler, J., and Nuttall, A. M.: Modeling the refreezing of meltwater as superimposed ice on a high Arctic glacier: a comparison of approaches, *J. Geophys. Res.*, 112, F04016, doi:10.1029/2007JF000818, 2007. 5108
- Zagorodnov, V., Sin'kevich, S., and Arkhipov, S.: Ice core express-analysis for structure and thermal regime studies of Austfonna, Mater. Glyatsiol. Issled./Data Glaciol. Stud., 66, 149–158, 1989 (in Russian with English summary). 5105
- Zwinger, T. and Moore, J. C.: Diagnostic and prognostic simulations with a full Stokes model accounting for superimposed ice of Midtre Lovénbreen, Svalbard, *The Cryosphere*, 3, 217–229, doi:10.5194/tc-3-217-2009, 2009. 5108, 5112
- Zwinger, T., Greve, R., Gagliardini, O., Shiraiwa, T., and Lyly, M.: A full Stokes-flow thermo-mechanical model for firn and ice applied to the Gorshkov crater glacier, Kamchatka, *Ann. Glaciol.*, 45, 29–37, 2007. 5105, 5107, 5119

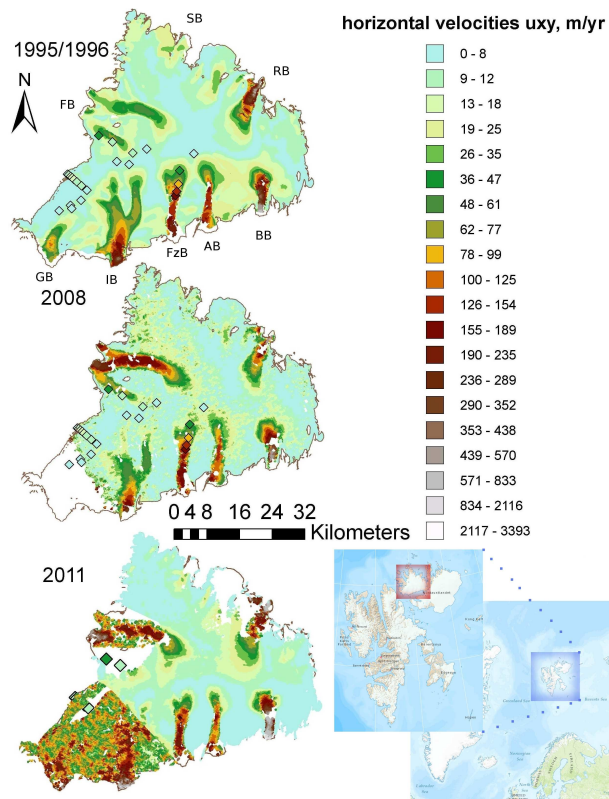


Fig. 1. Surface Velocities from remote sensing data in December/January 1995/96, December 2008 and December 2011 (original data). FB indicates the location of Franklinbreen, SB Sabinenbreen, RB Rijpbreen, BB Bodleybreen, AB Aldousbreen, FzB Frazerbreen, IB Idunbreen and GB Gimblebreen. In the lower right corner the location of Svalbard (blue square) and Vestfonna (red square) are shown.

Heat production sources and dynamics of VSF

M. Schäfer et al.

Title Page

Abstract Introduction

Conclusions References

Tables Figures

◀ ▶

◀ ▶

Back Close

Full Screen / Esc

Printer-friendly Version

Interactive Discussion



Heat production sources and dynamics of VSF

M. Schäfer et al.

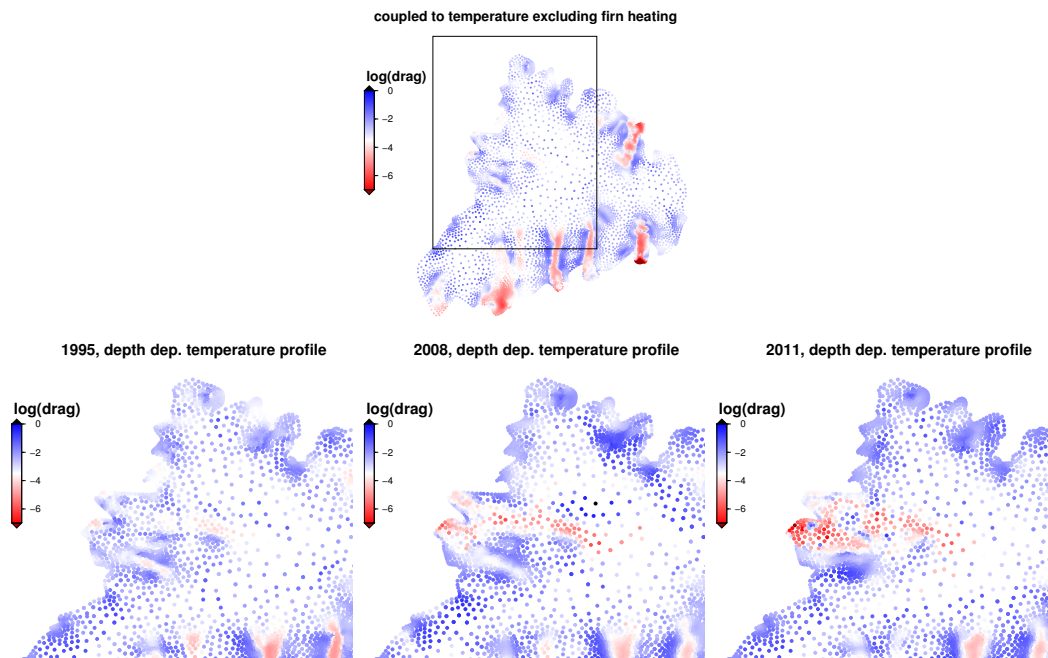


Fig. 2. Distribution of the basal drag coefficient in 1995 when coupling to temperature (upper line). The other three figures show a zoom over Franklinbreen (using the depth dependent temperature profile) in 1995, 2008 and 2011. Note that only the south-western corner has been patched with 1995 data in the 2008 and 2011 data sets. All figures are in logarithmic scale (units are MPa yr m^{-1}).

Title Page

Abstract

Introduction

Conclusions

References

Tables

Figures

◀

▶

◀

▶

Back

Close

Full Screen / Esc

Printer-friendly Version

Interactive Discussion



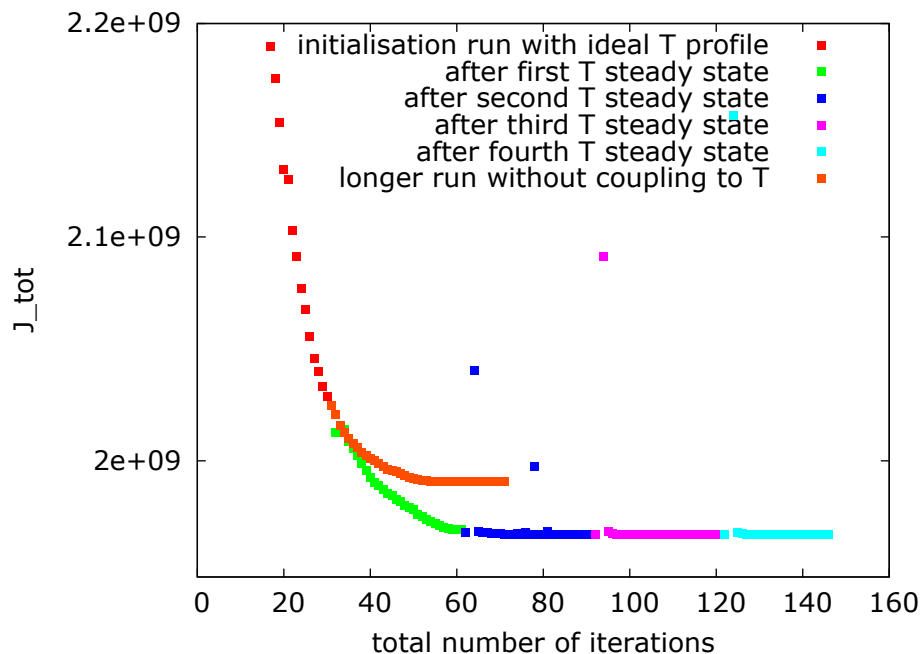


Fig. 3. Evolution of the total cost function J_{tot} (Eq. 17, log scale) when iterating inverse method and temperature steady-state calculation (1995 velocities). The graph is cut at 2.2×10^9 for better visibility, higher values in the first iterations are thus not visible. In orange the evolution of the cost function when not coupling with temperature is shown.

[Title Page](#)
[Abstract](#)
[Introduction](#)
[Conclusions](#)
[References](#)
[Tables](#)
[Figures](#)
[◀](#)
[▶](#)
[◀](#)
[▶](#)
[Back](#)
[Close](#)
[Full Screen / Esc](#)
[Printer-friendly Version](#)
[Interactive Discussion](#)


Heat production sources and dynamics of VSF

M. Schäfer et al.

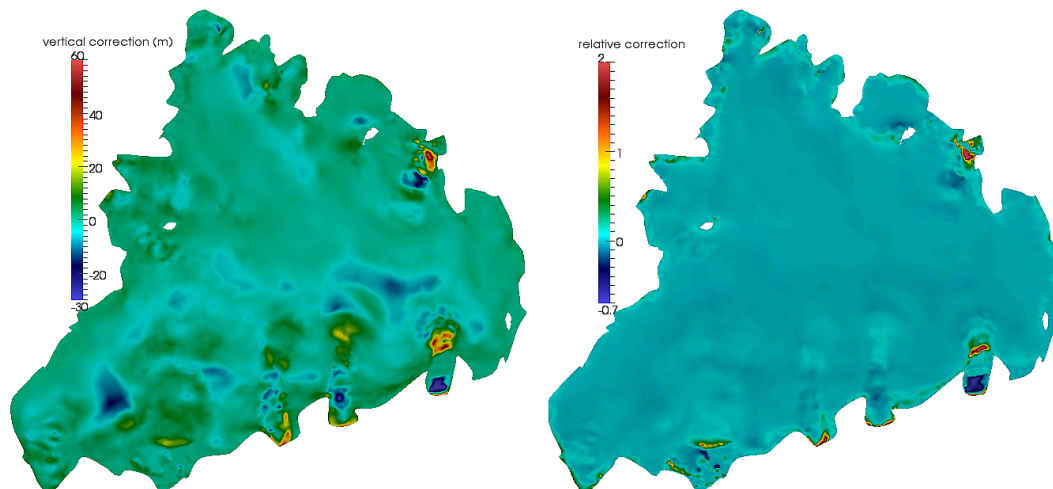


Fig. 4. Vertical corrections of the topographic data (1995 basal drag field) at the end of the initialization, to the left absolute corrections, to the right relative to the initial ice thickness.

[Title Page](#)[Abstract](#)[Introduction](#)[Conclusions](#)[References](#)[Tables](#)[Figures](#)[◀](#)[▶](#)[◀](#)[▶](#)[Back](#)[Close](#)[Full Screen / Esc](#)[Printer-friendly Version](#)[Interactive Discussion](#)

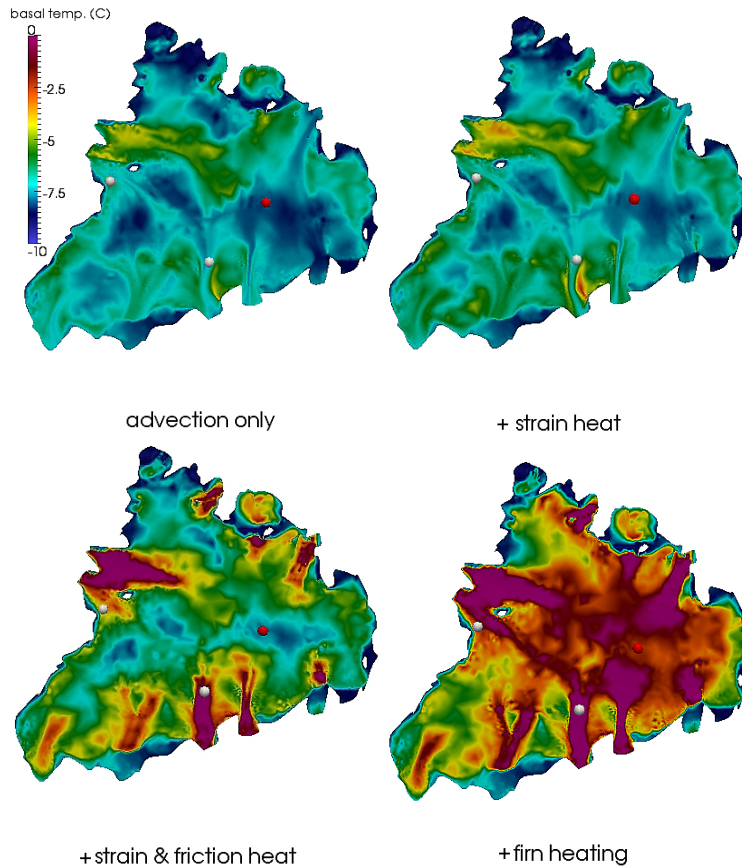


Fig. 5. Basal temperature field ($^{\circ}\text{C}$): (up left) advection only, (up right) adding of strain heating, (low left) adding of friction heating, (low right) adding of firn heating. The last figure remains unchanged whether the non-equilibrium part of the firn heating is added or not. The position of the ice core is indicated in red, the position of the two locations used in Fig. 6 in white.

Heat production sources and dynamics of VSF

M. Schäfer et al.

Title Page	
Abstract	Introduction
Conclusions	References
Tables	Figures
◀	▶
◀	▶
Back	Close
Full Screen / Esc	
Printer-friendly Version	
Interactive Discussion	



Heat production sources and dynamics of VSF

M. Schäfer et al.

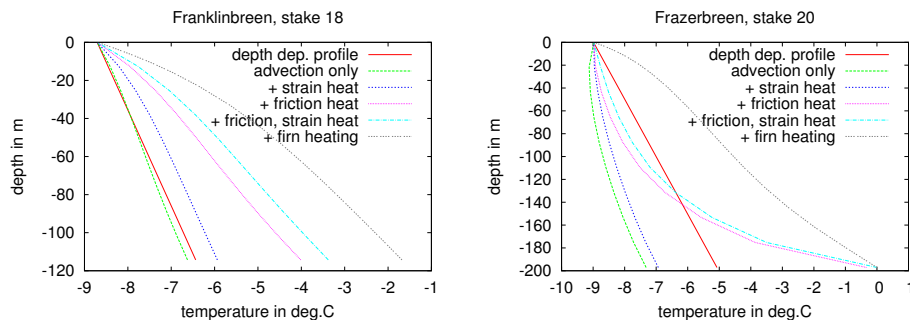


Fig. 6. Temperature profiles in chosen locations, (left) in the ablation zone of Franklinbreen and (right) in the accumulation zone of Frazerbreen: (1) depth dependent profile (Sect. 3.2) assumed in Schäfer et al. (2012) (red), (2) profile including advection, but no additional heat sources (green), (3) profile including advection and strain heating (blue), (4) profile including advection and friction heating (pink), (5) profile including advection and both strain and friction heating (light blue), (6) profile including also firn heating (gray), which is identical for the equilibrium state and the following 30 yr time-evolving simulation. The locations of these profiles are indicated in Fig. 5.

Title Page

Abstract

Introduction

Conclusions

References

Tables

Figures

◀

▶

◀

▶

Back

Close

Full Screen / Esc

Printer-friendly Version

Interactive Discussion



Heat production sources and dynamics of VSF

M. Schäfer et al.

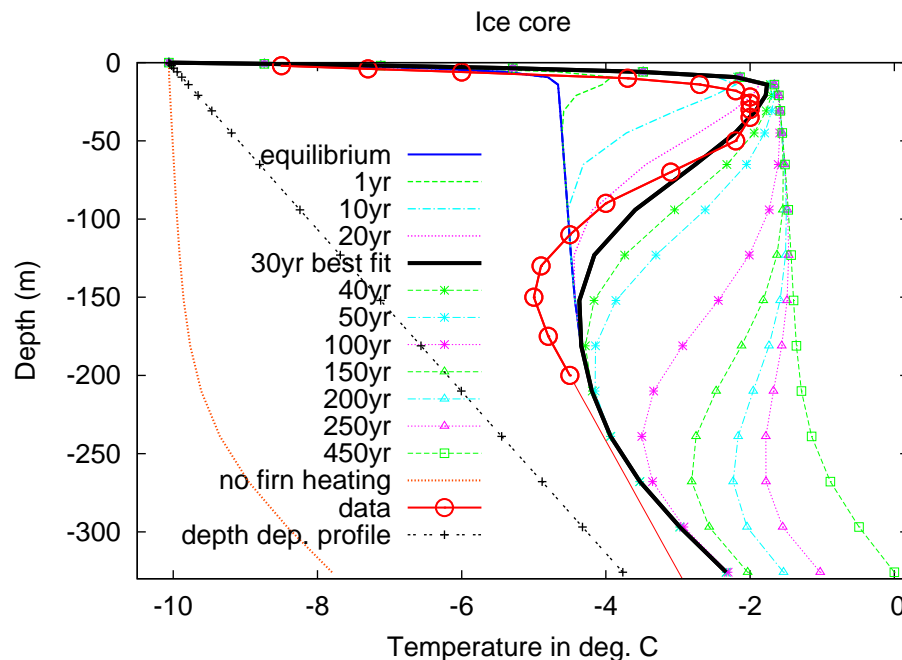


Fig. 7. Temperature profile as measured (red) in a drilling hole (Motoyama et al., 2008), the position is indicated in Fig. 5 (red dot). The dotted black line corresponds to the depth dependent profile, the brown line corresponds to the modeled temperature field including only strain and friction heating. The blue line is the result of the equilibrium firn heating simulation with the first set of parameters (percolation depth of 13.5 m). The green, cyan and pink profiles illustrate the evolution of temperature in the succeeding time evolving simulation with the second set of parameters (percolation depth of 18 m). The best fit to the data among these profiles after 30 yr is highlighted in black.

Title Page

Abstract

Introduction

Conclusions

References

Tables

Figures

◀

▶

◀

▶

Back

Close

Full Screen / Esc

Printer-friendly Version

Interactive Discussion



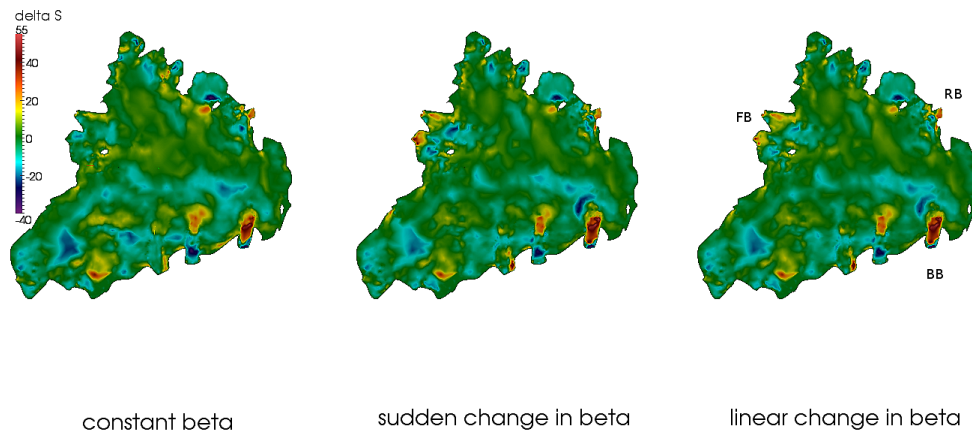


Fig. 8. Difference in change of surface elevation $\Delta S(m)$ during the prognostic 95–2008 simulation for the three scenarios: (1) constant basal drag coefficient, (2) sudden jump after 5 yr and (3) linear change in basal drag coefficient.

[Title Page](#)[Abstract](#)[Introduction](#)[Conclusions](#)[References](#)[Tables](#)[Figures](#)[◀](#)[▶](#)[◀](#)[▶](#)[Back](#)[Close](#)[Full Screen / Esc](#)[Printer-friendly Version](#)[Interactive Discussion](#)

Heat production sources and dynamics of VSF

M. Schäfer et al.

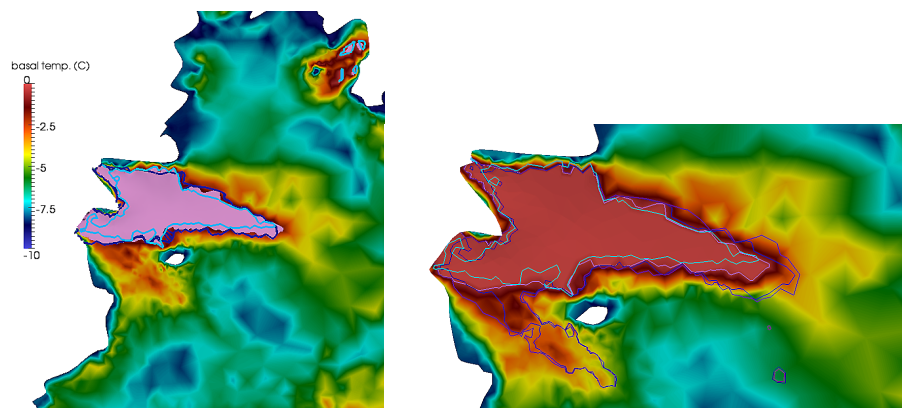


Fig. 9. In a zoom over the Franklinbreen area the change in the extent of the “sliding area” (basal temperatures above 272.5 K) is shown. To the left, light blue corresponds to the extent with the 1995 steady-state, dark blue to the 2008 steady-state and pink to the extent after the prognostic simulation. The temperature distribution in the background is the 1995ss temperature distribution. To the right, light colors present the “sliding area” when neglecting firn heating, dark colors when including it, blue lines represent the start of the 13 yr simulation and pink the value at the end. In the background the temperature at the end of the simulation when neglecting firn heating is drawn.

[Title Page](#)[Abstract](#)[Introduction](#)[Conclusions](#)[References](#)[Tables](#)[Figures](#)[◀](#)[▶](#)[◀](#)[▶](#)[Back](#)[Close](#)[Full Screen / Esc](#)[Printer-friendly Version](#)[Interactive Discussion](#)